



# ASTRO-H Space X-ray Observatory White Paper

## AGN Winds

J. S. Kaastra (SRON), Y. Terashima (Ehime University), T. Kallman (NASA/GSFC),  
Y. Haba (Aichi University of Education), E. Costantini (SRON), L. Gallo (Saint Mary's University),  
Y. Fukazawa (Hiroshima University), F. Tombesi (University of Maryland), N. Anabuki (Osaka University),  
H. Awaki (Ehime University), G. Brown (LLNL), L. di Gesu (SRON), K. Ebisawa (JAXA), J. Ebrero (SRON),  
M. Eckart (NASA/GSFC), K. Hagino (JAXA), K. S. Long (STScI), J. Miller (University of Michigan),  
T. Miyazawa (Nagoya University), S. Paltani (Université de Genève), C. Reynolds (University of Maryland),  
C. Ricci (Kyoto University), H. Sameshima (JAXA), H. Seta (Saitama University),  
Y. Ueda (Kyoto University), and M. Urry (Yale University)  
on behalf of the ASTRO-H Science Working Group

### Abstract

In this white paper we describe the prospects for *ASTRO-H* for the study of outflows from active galactic nuclei. The most important breakthroughs in this field are expected to arise from the high spectral resolution and sensitivity in the Fe-K band, combined with broad-band sensitivity over the full X-ray band and spectral capabilities also at lower energies. The sensitivity in the Fe-K region allows to extend the absorption measure distribution of the outflow out to the highest ionisation states accessible, where observations with current X-ray missions indicate that most of the outflowing gas is to be found. Due to the high-resolution and sensitivity it will also be able to give the definitive proof for the existence of ultra-fast outflows, and if so, characterise their physical properties in great detail. These ultra-fast outflows carry very large amounts of energy and momentum, and are of fundamental importance for feedback studies. We show how the *ASTRO-H* observations in general can help to constrain numerical models for outflows. The link to reflection and emission processes is also discussed, as well as the possible relation between outflows and relativistic emission lines. Finally, we discuss the prospects for other related categories of objects like BAL quasars, partially covered sources and Compton thick outflows.

## Complete list of the ASTRO-H Science Working Group

Tadayuki Takahashi<sup>a</sup>, Kazuhisa Mitsuda<sup>a</sup>, Richard Kelley<sup>b</sup>, Felix Aharonian<sup>c</sup>, Hiroki Akamatsu<sup>d</sup>, Fumie Akimoto<sup>e</sup>, Steve Allen<sup>f</sup>, Naohisa Anabuki<sup>g</sup>, Lorella Angelini<sup>b</sup>, Keith Arnaud<sup>b</sup>, Marc Audard<sup>i</sup>, Hisamitsu Awaki<sup>j</sup>, Aya Bamba<sup>k</sup>, Marshall Bautz<sup>l</sup>, Roger Blandford<sup>f</sup>, Laura Brenneman<sup>b</sup>, Greg Brown<sup>m</sup>, Edward Cackett<sup>n</sup>, Maria Chernyakova<sup>c</sup>, Meng Chiao<sup>b</sup>, Paolo Coppi<sup>o</sup>, Elisa Costantini<sup>d</sup>, Jelle de Plaa<sup>d</sup>, Jan-Willem den Herder<sup>d</sup>, Chris Done<sup>p</sup>, Tadayasu Dotani<sup>a</sup>, Ken Ebisawa<sup>a</sup>, Megan Eckart<sup>b</sup>, Teruaki Enoto<sup>q</sup>, Yuichiro Ezoe<sup>r</sup>, Andrew Fabian<sup>n</sup>, Carlo Ferrigno<sup>i</sup>, Adam Foster<sup>s</sup>, Ryuichi Fujimoto<sup>t</sup>, Yasushi Fukazawa<sup>u</sup>, Stefan Funk<sup>f</sup>, Akihiro Furuzawa<sup>e</sup>, Massimiliano Galeazzi<sup>v</sup>, Luigi Gallo<sup>w</sup>, Poshak Gandhi<sup>p</sup>, Matteo Guainazzi<sup>x</sup>, Yoshito Haba<sup>y</sup>, Kenji Hamaguchi<sup>h</sup>, Isamu Hatsukade<sup>z</sup>, Takayuki Hayashi<sup>a</sup>, Katsuhiro Hayashi<sup>a</sup>, Kiyoshi Hayashida<sup>g</sup>, Junko Hiraga<sup>aa</sup>, Ann Hornschemeier<sup>b</sup>, Akio Hoshino<sup>ab</sup>, John Hughes<sup>ac</sup>, Una Hwang<sup>ad</sup>, Ryo Iizuka<sup>a</sup>, Yoshiyuki Inoue<sup>a</sup>, Hajime Inoue<sup>a</sup>, Kazunori Ishibashi<sup>e</sup>, Manabu Ishida<sup>a</sup>, Kumi Ishikawa<sup>q</sup>, Yoshitaka Ishisaki<sup>f</sup>, Masayuki Ito<sup>ae</sup>, Naoko Iyomoto<sup>af</sup>, Jelle Kaastra<sup>d</sup>, Timothy Kallman<sup>b</sup>, Tuneyoshi Kamae<sup>f</sup>, Jun Kataoka<sup>ag</sup>, Satoru Katsuda<sup>a</sup>, Junichiro Katsuta<sup>u</sup>, Madoka Kawaharada<sup>a</sup>, Nobuyuki Kawai<sup>ah</sup>, Dmitry Khangulyan<sup>a</sup>, Caroline Kilbourne<sup>b</sup>, Masashi Kimura<sup>ai</sup>, Shunji Kitamoto<sup>ab</sup>, Tetsu Kitayama<sup>aj</sup>, Takayoshi Kohmura<sup>ak</sup>, Motohide Kokubun<sup>a</sup>, Saori Konami<sup>r</sup>, Katsuji Koyama<sup>al</sup>, Hans Krimm<sup>b</sup>, Aya Kubota<sup>am</sup>, Hideyo Kunieda<sup>e</sup>, Stephanie LaMassa<sup>o</sup>, Philippe Laurent<sup>an</sup>, François Lebrun<sup>an</sup>, Maurice Leutenegger<sup>b</sup>, Olivier Limousin<sup>an</sup>, Michael Loewenstein<sup>b</sup>, Knox Long<sup>ao</sup>, David Lumb<sup>ap</sup>, Grzegorz Madejski<sup>f</sup>, Yoshitomo Maeda<sup>a</sup>, Kazuo Makishima<sup>aa</sup>, Maxim Markevitch<sup>b</sup>, Hironori Matsumoto<sup>e</sup>, Kyoko Matsushita<sup>aq</sup>, Dan McCammon<sup>af</sup>, Brian McNamara<sup>as</sup>, Jon Miller<sup>at</sup>, Eric Miller<sup>l</sup>, Shin Mineshige<sup>au</sup>, Ikuyuki Mitsuishi<sup>e</sup>, Takuya Miyazawa<sup>e</sup>, Tsunefumi Mizuno<sup>u</sup>, Koji Mori<sup>z</sup>, Hideyuki Mori<sup>e</sup>, Koji Mukai<sup>b</sup>, Hiroshi Murakami<sup>av</sup>, Toshio Murakami<sup>t</sup>, Richard Mushotzky<sup>h</sup>, Ryo Nagino<sup>g</sup>, Takao Nakagawa<sup>a</sup>, Hiroshi Nakajima<sup>g</sup>, Takeshi Nakamori<sup>aw</sup>, Shinya Nakashima<sup>a</sup>, Kazuhiro Nakazawa<sup>aa</sup>, Masayoshi Nobukawa<sup>al</sup>, Hirofumi Noda<sup>q</sup>, Masaharu Nomachi<sup>ax</sup>, Steve O' Dell<sup>ay</sup>, Hirokazu Odaka<sup>a</sup>, Takaya Ohashi<sup>r</sup>, Masanori Ohno<sup>u</sup>, Takashi Okajima<sup>b</sup>, Naomi Ota<sup>az</sup>, Masanobu Ozaki<sup>a</sup>, Frits Paerels<sup>ba</sup>, Stéphane Paltani<sup>i</sup>, Arvind Parmar<sup>x</sup>, Robert Petre<sup>b</sup>, Ciro Pinto<sup>n</sup>, Martin Pohl<sup>i</sup>, F. Scott Porter<sup>b</sup>, Katja Pottschmidt<sup>b</sup>, Brian Ramsey<sup>ay</sup>, Rubens Reis<sup>at</sup>, Christopher Reynolds<sup>h</sup>, Claudio Ricci<sup>au</sup>, Helen Russell<sup>n</sup>, Samar Safi-Harb<sup>bb</sup>, Shinya Saito<sup>a</sup>, Hiroaki Sameshima<sup>a</sup>, Goro Sato<sup>ag</sup>, Kosuke Sato<sup>aq</sup>, Rie Sato<sup>a</sup>, Makoto Sawada<sup>k</sup>, Peter Serlemitsos<sup>b</sup>, Hiromi Seta<sup>bc</sup>, Aurora Simionescu<sup>a</sup>, Randall Smith<sup>s</sup>, Yang Soong<sup>b</sup>, Łukasz Stawarz<sup>a</sup>, Yasuharu Sugawara<sup>bd</sup>, Satoshi Sugita<sup>j</sup>, Andrew Szymkowiak<sup>o</sup>, Hiroyasu Tajima<sup>e</sup>, Hiromitsu Takahashi<sup>u</sup>, Hiroaki Takahashi<sup>g</sup>, Yoh Takei<sup>a</sup>, Toru Tamagawa<sup>q</sup>, Takayuki Tamura<sup>a</sup>, Keisuke Tamura<sup>e</sup>, Takaaki Tanaka<sup>al</sup>, Yasuo Tanaka<sup>a</sup>, Yasuyuki Tanaka<sup>u</sup>, Makoto Tashiro<sup>bc</sup>, Yuzuru Tawara<sup>e</sup>, Yukikatsu Terada<sup>bc</sup>, Yuichi Terashima<sup>j</sup>, Francesco Tombesi<sup>b</sup>, Hiroshi Tomida<sup>ai</sup>, Yohko Tsuboi<sup>bd</sup>, Masahiro Tsujimoto<sup>a</sup>, Hiroshi Tsunemi<sup>g</sup>, Takeshi Tsuru<sup>al</sup>, Hiroyuki Uchida<sup>al</sup>, Yasunobu Uchiyama<sup>ab</sup>, Hideki Uchiyama<sup>be</sup>, Yoshihiro Ueda<sup>au</sup>, Shutaro Ueda<sup>g</sup>, Shiro Ueno<sup>ai</sup>, Shinichiro Uno<sup>bf</sup>, Meg Urry<sup>o</sup>, Eugenio Ursino<sup>v</sup>, Cor de Vries<sup>d</sup>, Shin Watanabe<sup>a</sup>, Norbert Werner<sup>f</sup>, Dan Wilkins<sup>w</sup>, Shinya Yamada<sup>r</sup>, Hiroya Yamaguchi<sup>b</sup>, Kazutaka Yamaoka<sup>e</sup>, Noriko Yamasaki<sup>a</sup>, Makoto Yamauchi<sup>z</sup>, Shigeo Yamauchi<sup>az</sup>, Tahir Yaqoob<sup>b</sup>, Yoichi Yatsu<sup>ah</sup>, Daisuke Yonetoku<sup>t</sup>, Atsumasa Yoshida<sup>k</sup>, Takayuki Yuasa<sup>q</sup>, Irina Zhuravleva<sup>f</sup>, Abderahmen Zoghbi<sup>h</sup>, and John ZuHone<sup>b</sup>

<sup>a</sup>Institute of Space and Astronautical Science (ISAS), Japan Aerospace Exploration Agency (JAXA), Kanagawa 252-5210, Japan

<sup>b</sup>NASA/Goddard Space Flight Center, MD 20771, USA

<sup>c</sup>Astronomy and Astrophysics Section, Dublin Institute for Advanced Studies, Dublin 2, Ireland

<sup>d</sup>SRON Netherlands Institute for Space Research, Utrecht, The Netherlands

<sup>e</sup>Department of Physics, Nagoya University, Aichi 338-8570, Japan

<sup>f</sup>Kavli Institute for Particle Astrophysics and Cosmology, Stanford University, CA 94305, USA

<sup>g</sup>Department of Earth and Space Science, Osaka University, Osaka 560-0043, Japan

<sup>h</sup>Department of Astronomy, University of Maryland, MD 20742, USA

<sup>i</sup>Université de Genève, Genève 4, Switzerland

<sup>j</sup>Department of Physics, Ehime University, Ehime 790-8577, Japan

<sup>k</sup>Department of Physics and Mathematics, Aoyama Gakuin University, Kanagawa 229-8558, Japan

<sup>l</sup>Kavli Institute for Astrophysics and Space Research, Massachusetts Institute of Technology, MA 02139, USA

<sup>m</sup>Lawrence Livermore National Laboratory, CA 94550, USA

<sup>n</sup>Institute of Astronomy, Cambridge University, CB3 0HA, UK

<sup>o</sup>Yale Center for Astronomy and Astrophysics, Yale University, CT 06520-8121, USA

<sup>p</sup>Department of Physics, University of Durham, DH1 3LE, UK

<sup>q</sup>RIKEN, Saitama 351-0198, Japan

<sup>r</sup>Department of Physics, Tokyo Metropolitan University, Tokyo 192-0397, Japan

<sup>s</sup>Harvard-Smithsonian Center for Astrophysics, MA 02138, USA

- <sup>t</sup>Faculty of Mathematics and Physics, Kanazawa University, Ishikawa 920-1192, Japan
- <sup>u</sup>Department of Physical Science, Hiroshima University, Hiroshima 739-8526, Japan
- <sup>v</sup>Physics Department, University of Miami, FL 33124, USA
- <sup>w</sup>Department of Astronomy and Physics, Saint Mary's University, Nova Scotia B3H 3C3, Canada
- <sup>x</sup>European Space Agency (ESA), European Space Astronomy Centre (ESAC), Madrid, Spain
- <sup>y</sup>Department of Physics and Astronomy, Aichi University of Education, Aichi 448-8543, Japan
- <sup>z</sup>Department of Applied Physics, University of Miyazaki, Miyazaki 889-2192, Japan
- <sup>aa</sup>Department of Physics, University of Tokyo, Tokyo 113-0033, Japan
- <sup>ab</sup>Department of Physics, Rikkyo University, Tokyo 171-8501, Japan
- <sup>ac</sup>Department of Physics and Astronomy, Rutgers University, NJ 08854-8019, USA
- <sup>ad</sup>Department of Physics and Astronomy, Johns Hopkins University, MD 21218, USA
- <sup>ae</sup>Faculty of Human Development, Kobe University, Hyogo 657-8501, Japan
- <sup>af</sup>Kyushu University, Fukuoka 819-0395, Japan
- <sup>ag</sup>Research Institute for Science and Engineering, Waseda University, Tokyo 169-8555, Japan
- <sup>ah</sup>Department of Physics, Tokyo Institute of Technology, Tokyo 152-8551, Japan
- <sup>ai</sup>Tsukuba Space Center (TKSC), Japan Aerospace Exploration Agency (JAXA), Ibaraki 305-8505, Japan
- <sup>aj</sup>Department of Physics, Toho University, Chiba 274-8510, Japan
- <sup>ak</sup>Department of Physics, Tokyo University of Science, Chiba 278-8510, Japan
- <sup>al</sup>Department of Physics, Kyoto University, Kyoto 606-8502, Japan
- <sup>am</sup>Department of Electronic Information Systems, Shibaura Institute of Technology, Saitama 337-8570, Japan
- <sup>an</sup>IRFU/Service d'Astrophysique, CEA Saclay, 91191 Gif-sur-Yvette Cedex, France
- <sup>ao</sup>Space Telescope Science Institute, MD 21218, USA
- <sup>ap</sup>European Space Agency (ESA), European Space Research and Technology Centre (ESTEC), 2200 AG Noordwijk, The Netherlands
- <sup>aq</sup>Department of Physics, Tokyo University of Science, Tokyo 162-8601, Japan
- <sup>ar</sup>Department of Physics, University of Wisconsin, WI 53706, USA
- <sup>as</sup>University of Waterloo, Ontario N2L 3G1, Canada
- <sup>at</sup>Department of Astronomy, University of Michigan, MI 48109, USA
- <sup>au</sup>Department of Astronomy, Kyoto University, Kyoto 606-8502, Japan
- <sup>av</sup>Department of Information Science, Faculty of Liberal Arts, Tohoku Gakuin University, Miyagi 981-3193, Japan
- <sup>aw</sup>Department of Physics, Faculty of Science, Yamagata University, Yamagata 990-8560, Japan
- <sup>ax</sup>Laboratory of Nuclear Studies, Osaka University, Osaka 560-0043, Japan
- <sup>ay</sup>NASA/Marshall Space Flight Center, AL 35812, USA
- <sup>az</sup>Department of Physics, Faculty of Science, Nara Women's University, Nara 630-8506, Japan
- <sup>ba</sup>Department of Astronomy, Columbia University, NY 10027, USA
- <sup>bb</sup>Department of Physics and Astronomy, University of Manitoba, MB R3T 2N2, Canada
- <sup>bc</sup>Department of Physics, Saitama University, Saitama 338-8570, Japan
- <sup>bd</sup>Department of Physics, Chuo University, Tokyo 112-8551, Japan
- <sup>be</sup>Science Education, Faculty of Education, Shizuoka University, Shizuoka 422-8529, Japan
- <sup>bf</sup>Faculty of Social and Information Sciences, Nihon Fukushi University, Aichi 475-0012, Japan

# Contents

<b>1</b>	<b>High-ionisation gas in “normal” outflows</b>	<b>5</b>
1.1	Background and Previous Studies . . . . .	5
1.2	Prospects & Strategy . . . . .	6
1.2.1	Absorption line detection . . . . .	7
1.2.2	Practical example . . . . .	8
1.3	Targets & Feasibility . . . . .	8
1.3.1	NGC 4151 . . . . .	10
1.3.2	NGC 3783 . . . . .	10
1.3.3	NGC 5548 . . . . .	11
1.3.4	NGC 3516 . . . . .	12
1.3.5	H 0557-385 . . . . .	14
1.4	Beyond Feasibility . . . . .	14
<b>2</b>	<b>Ultra Fast Outflows</b>	<b>14</b>
2.1	Background and Previous Studies . . . . .	14
2.2	Prospects & Strategy . . . . .	16
2.3	Targets & Feasibility . . . . .	17
2.3.1	Mrk 509 . . . . .	18
2.3.2	3C 111 . . . . .	18
2.3.3	PG 1211+143 . . . . .	19
<b>3</b>	<b>Comparison with numerical models</b>	<b>20</b>
3.1	Background and Previous Studies . . . . .	20
3.2	Prospects & Strategy . . . . .	21
3.3	Targets & Feasibility . . . . .	22
<b>4</b>	<b>Other types of sources with potential (narrow-band) outflow features</b>	<b>22</b>
4.1	Background and Previous Studies . . . . .	22
4.1.1	BAL quasars . . . . .	22
4.1.2	Partially covered sources . . . . .	23
4.1.3	Compton thick outflows . . . . .	23
4.2	Prospects & Strategy . . . . .	23
4.3	Targets & Feasibility . . . . .	24
4.3.1	BAL QSOs . . . . .	24
4.3.2	Compton thick outflows . . . . .	24

# 1 High-ionisation gas in “normal” outflows

## 1.1 Background and Previous Studies

It has been recognised over the past years that AGN play a fundamental role in a broad range of astrophysical processes. There is a tight relation between the growth of the black holes and the evolution of the host galaxy, and feedback processes between outflows from the black hole surroundings with their environment may regulate this. The strongest feedback occurs for the supermassive black holes at the centres of giant cD galaxies in cluster centres, where the effects of the AGN activity in its “radio mode” can be felt up to Mpc-scale distances. These cases are treated in detail in the cluster sections of this white paper.

Here we focus on the outflows from “normal” AGN in their quasar mode. The presence of outflows was first discovered from optical and UV spectra of AGN. Evidence for photo-ionised gas surrounding the nucleus and giving rise to X-ray absorption as visible through absorption edges of in particular O VII and O VIII was first inferred from *ROSAT* PSPC data, although the credit of the first discovery goes to Halpern (1984), who inferred the presence of photo-ionised gas in MR 2251–178 using *Einstein* MPC data. With the availability of CCDs through the launch of *ASCA*, the absorption edges from the so-called warm absorbers were readily discovered and analysed for large samples of AGN (see Reynolds, 1997, for an example).

Subsequently, when the first X-ray grating spectrometers were launched (*Chandra* with the High Energy Transmission Grating Spectrometer, HETG, and Low Energy Transmission Grating Spectrometer, LETG, and *XMM-Newton* with the Reflection Grating Spectrometers, RGS), it was found that also line absorption plays an important role, and that the warm absorbers show blueshifts, indicating that they are outflowing. This was already clear from the first high-resolution X-ray spectrum, taken with the LETG of the Seyfert galaxy NGC 5548 (Kaastra et al., 2000), and confirmed soon after in NGC 3783 (Kaspi et al., 2000).

Based on a large number of papers that appeared in the literature since then, the following picture arises. Outflows are seen in X-rays in about half of all the type 1 sources, which is usually being interpreted that they cover about half of the available solid angle of the ionisation cone. This is not necessarily true if the outflow has significant bending due to e.g. ongoing acceleration. Observations and modeling of UV lines in emission shows that the column density rises for increasing inclination angle of the AGN (Fischer et al., 2012), and showing a smooth transition towards type 2 sources, indicating that the outflows may be stronger near the torus than the AGN axis.

Outflow velocities usually range between almost zero, to common values of a few hundred  $\text{km s}^{-1}$  up to a few  $1000 \text{ km s}^{-1}$  in some cases (ultra-fast outflows are discussed later). The number of components seen ranges between one up to several, and usually the UV spectra have the best resolving power to separate the different dynamical components, but they are by nature limited to the lowly-ionised gas. In many cases, however, there is a clear connection between the UV absorption components and the X-ray absorption components.

When we consider the ionisation structure of the outflow, already the first LETG spectrum of an AGN outflow showed evidence for at least three ionisation components (Kaastra et al., 2002). With more data available, the debate was arising whether the absorption measure distribution (AMD), the function describing the column density  $N_{\text{H}}$  as a function of ionisation parameter  $\xi$ , is continuous or not. One point of view is that the AMD is power-law like over three orders of magnitude in  $\xi$  (Steenbrugge et al., 2005). Another point of view is that the AMD has discrete components and that these components are in pressure equilibrium (Krongold et al., 2003). Recently, very deep observations of Mrk 509 showed that the AMD indeed has discrete components, but these are not in pressure equilibrium (Detmers et al., 2011). See also Figure 1.

Different origins for the outflow have been proposed, like accretion disk winds, thermal evaporation from the torus, or extended ionisation cones. These models all imply very different effects for the impact of the outflow on the environment, the feedback process. First, outflows launched close to the black hole (like accretion disk winds) have to overcome a larger gravitational potential to escape, hence should have much larger outflow velocities  $v$ , from thousands of km/s to significant fractions of the speed of light. Furthermore, outflows at larger distances  $r$  from the black hole (like e.g. torus winds) have a larger impact on the surroundings, because we have for the mass loss rate  $\dot{M}$ :

$$\dot{M}/\Omega = N_{\text{H}}m_p r v, \quad (1)$$

with  $\Omega$  the solid angle subtended by the outflow,  $m_p$  the proton mass and  $N_H$  the total column density (dominated by hydrogen). The kinetic luminosity  $L_K$  is simply given by  $\frac{1}{2}\dot{M}v^2$ . Thus, the fastest winds generally dump most energy into their surroundings, and therefore they are of most interest for studies of cosmic feedback.

Empirically, it is not easy to determine the location of the outflow, because the spectrum only yields the physical state (from the ions that are present and line broadening), the total column density (from the depth of the lines) and the outflow velocity (from the Doppler shift of the lines). However, because the ionisation parameter  $\xi$  is given by

$$\xi = L/nr^2 \quad (2)$$

with  $L$  the ionising luminosity,  $n$  the hydrogen density and  $r$  the distance of the gas from the central black hole, a density measurement would yield directly the distance, because both  $L$  and  $\xi$  can be deduced directly from the spectrum.  $\xi$  is usually expressed in units of  $\text{erg s}^{-1} \text{cm}$  or  $10^{-9} \text{Wm}$ , which is used throughout this paper. The density can sometimes be obtained using UV absorption lines from meta-stable levels, for the lowly ionised gas components, or through measuring the response of the outflow to variations in the ionising continuum (i.e., measuring the recombination time scale which is proportional to  $1/n$ ). The latter method requires monitoring of a source at regular intervals, and has been applied successfully to Mrk 509 (Kaastra et al., 2012). In the latter case it was found that the dominant X-ray absorption components are located at a distance of a few to a few tens of pc from the nucleus, near the inner parts of the torus.

Interestingly, several AGN show a tendency of increasing outflow velocity as a function of ionisation parameter (Steenbrugge et al., 2005; Tombesi et al., 2013). A major uncertainty, however, is how this trend continues to higher ionisation parameter (say  $\log \xi > 3$ ), and in addition, how the AMD behaves at high ionisation parameter. At lower ionisation parameter, the AMD, defined as

$$\text{AMD} = \xi dN_H/d\xi \quad (3)$$

increases approximately as a power law function of  $\log \xi$  (at the discrete  $\xi$ -values where it is non-zero), with power-law index typically 0.0 – 0.4, (cf. Behar, 2009). Thus, there is more gas at higher ionisation parameter, unless of course there would be a natural cut-off to the AMD.

## 1.2 Prospects & Strategy

The increase of the AMD towards higher ionisation parameter, as well as the tendency of higher outflow velocities at higher ionisation parameter, offer unique prospects for *ASTRO-H* to study AGN outflows, because this may imply that the dynamically most important part of the outflow occurs at these high values of  $\xi$ . Observationally, the highest ionised gas components are best studied by measuring the K-shell transitions of Fe XXV and Fe XXVI.

We note here that the Fe-K band also contains strong absorption features from transitions of Li-like Fe and higher iso-electronic sequences, and *ASTRO-H* measurements will definitely make use of these last types of transitions. However, the same ions have also transitions in the L-band near 1 keV, also detectable by SXS, but in that energy band the grating spectrometers of *Chandra* and *XMM-Newton* are getting more sensitive and have already explored quite well parameter space (see the introduction before). Therefore, here we focus uniquely on the prospects for discoveries based on Fe XXV and Fe XXVI. However, we note here that in the same spectral region, for very well exposed spectra, also the equivalent nickel lines will become accessible.

We first consider the stability curve of photo-ionisation equilibrium and the different discrete phases. Figure 1 shows the photo-ionisation equilibrium curve for Mrk 509 with the discrete components found by Detmers et al. (2011). It is seen that we expect Fe XXV and Fe XXVI to peak around the position of the last unstable branch, and in the latter case already on the stable Compton branch. Measuring the column density, outflow velocity, turbulence and other parameters for these ions therefore will provide us unique insight into the dynamically most important component of the outflow. Even a non-detection would give extremely useful upper limits.

Up to now, there have been two clear cases of absorption line detections in the Fe-K band. One case is NGC 3783, where Reeves et al. (2004) found evidence ( $4.5\sigma$ ) for the Fe XXV 1s–2p absorption line in a deep *XMM-Newton* EPIC spectrum. There was evidence for variability on a  $10^5$  s time scale. NGC 3783 is an

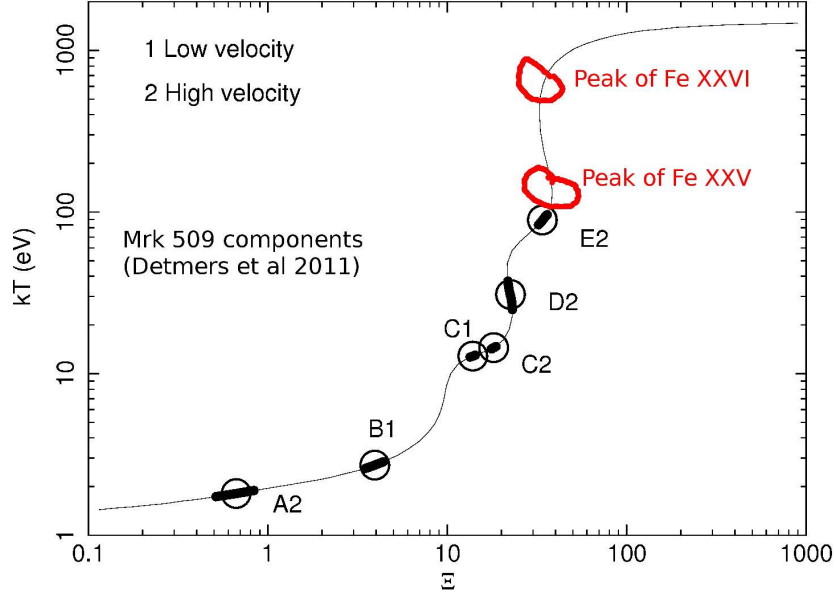


**Figure 1:** Photoionisation equilibrium curve for Mrk 509, based on Detmers et al. (2011). Components are in pressure equilibrium when they share the same value of  $\Xi \equiv \xi/4\pi ckT$ . Stable equilibrium only exists on parts of the curve with positive slope. The discrete components found by Detmers et al. are indicated by circles and labels corresponding to the designation in that paper, and the thick parts on the curve correspond to the measured uncertainty in the ionisation parameter  $\xi$  for these components. In red we indicate at which parts of the curve Fe XXV and Fe XXVI are expected to peak.

AGN with one of the highest outflow column densities, explaining why a limited detection with a CCD camera was possible. The other case is the deep 520 ks *Chandra* HETG spectrum of MCG –6-30-15, showing H-like and He-like Fe absorption lines outflowing at 2000 km s<sup>-1</sup> at a very high column density of 10<sup>23.2</sup> cm<sup>-2</sup> at log  $\xi$  = 3.6 (Young et al., 2005).

As we will show, it is not very hard to get line detections with SXS, but in order to constrain the physical parameters we need better quality spectra hence longer exposure times. This will be elaborated in the next section. It is important to get a well-justified sample of sources spanning a broad range of parameters, from low mass narrow-line Seyfert galaxies to high-mass quasars, and preferably also with other different parameters such as column density of the outflow, different ionising spectral energy distributions, etc.

Before proceeding, however, we first make some basic estimates that help to prepare the source selection.

### 1.2.1 Absorption line detection

Here we provide a few simple estimates of what column densities can be detected with SXS in the Fe-K band. Starting point is a power-law continuum with effective photon index 1.7 and 2–10 keV flux  $F$  of 5 units (one unit is here 10<sup>-14</sup> W m<sup>-2</sup> or 10<sup>-11</sup> erg cm<sup>-2</sup> s<sup>-1</sup>). This is the typical flux of one of the brighter Seyfert galaxies. We consider a canonical exposure time  $t$  of 100 ks, and the SXS effective area  $A(E)$ , with spectral resolution  $\Delta E = 5$  eV. Let the equivalent width of the line be  $W$ . If the line is weak,  $W \ll \Delta E$ , and if the line is strong,  $W \gg \Delta E$ .

For any line, the number of continuum counts  $N_c$  acting as “background” for line detection is:

$$N_c = A(E) t F(E) W_{\text{eff}}, \quad (4)$$

where  $F(E)$  is photon flux in photons area<sup>-1</sup> time<sup>-1</sup> energy<sup>-1</sup>, and

$$\text{Weak line: } W_{\text{eff}} = \Delta E, \quad (5)$$

$$\text{Strong line: } W_{\text{eff}} = W. \quad (6)$$

The number of line photons  $N_l$  taken away from the continuum is

$$N_l = A(E) t F(E) W. \quad (7)$$

The signal to noise ratio S/N of the detection (“number of sigma’s” or  $n\sigma$  of the detection) is given by

$$\text{weak line: } S/N = N_l / \sqrt{N_c} = \sqrt{A(E) t F(E)} W / \sqrt{\Delta E}. \quad (8)$$

For a strong absorption line, it is essentially provided by the uncertainty in the number of continuum photons that are absorbed (assuming a “black” line):

$$\text{strong line: } S/N = \sqrt{N_c} = \sqrt{A(E) t F(E)} \sqrt{W}. \quad (9)$$

These results can be generalised to

$$S/N = \sqrt{A(E) t F(E)} \frac{W}{\sqrt{\max(\Delta E, W)}}. \quad (10)$$

### 1.2.2 Practical example

The above formalism has been applied to absorption lines from a few ions: the Fe XXVI Lyman  $\alpha$  and  $\beta$  lines (1s–2p and 1s–3p), the Fe XXV 1s–2p and 1s–3p lines, the Fe XXIV q, r and t lines, and the strongest Fe XXIV line in the Fe-L band. Figure 2 shows the significance of line detection for different values of the Gaussian velocity dispersion  $\sigma$  as indicated.

For Solar abundances, the maximum concentrations that the ions Fe XXIV, Fe XXV and Fe XXVI relative to hydrogen can reach, are  $6 \times 10^{-6}$ ,  $1.7 \times 10^{-5}$ , and  $1.5 \times 10^{-5}$  respectively.

Thus, for instance, to detect the strong Fe XXV resonance line at 6.7 keV: from the figure we see that the  $3\sigma$  detection limit is reached for an ionic column density of about  $2 - 4 \times 10^{20} \text{ m}^{-2}$ , depending upon the velocity dispersion, and thus the minimum equivalent hydrogen column density (for Solar abundances) is  $1 - 2 \times 10^{25} \text{ m}^{-2}$  ( $1 - 2 \times 10^{21} \text{ cm}^{-2}$ ). Such columns are not very large and easily detectable. However, note the scaling with source flux: for a ten times weaker source, the minimum detectable column density may be two orders of magnitude larger.

## 1.3 Targets & Feasibility

We have selected targets starting from a few review papers. We have chosen here the reviews by Blustin et al. (2005), McKernan et al. (2007) and Tombesi et al. (2012). From these, we took 23 sources with measured  $\xi$  and column density. When multiple components were given, we took the one with the highest ionisation parameter. We estimated equivalent hydrogen columns for Fe XXV and Fe XXVI by assuming they peak at  $\log \xi$  values of 3.7 and 4.1, respectively (these values are appropriate for Mrk 509). We then scaled column densities to these values by scaling with  $\xi^{0.2}$ , a typical value found by Behar (2009). Median 2–10 keV fluxes were taken from two sources: the Tombesi et al. (2010a) paper and a private list of 2–10 keV fluxes from various satellites in the pre-ASCA era.

For each of these sources, we simulated the spectrum using a power law with photon index 1.7 and the appropriate 2–10 keV flux, with the absorption by Fe XXV and Fe XXVI calculated through the *slab* model of SPEX, which calculates the opacity for each individual ion. A uniform Gaussian velocity broadening of  $\sigma = 100 \text{ km s}^{-1}$  was adopted. We then simulated these spectra for SXS using 500 ks exposure time and determined the accuracy of the measured column densities. The relative uncertainties on the measured ionic column densities were inverted to get the equivalent number of sigmas for the significance. We found a dozen sources where a  $5\sigma$  detection for both ions within 500 ks is possible.

One needs to take care, however, in selecting sources based on such simulations. For instance, for MCG 8-11-11 it appears that the initial high column density ( $N_H = 10^{22} \text{ cm}^{-2}$ ) found by Matt et al. (2006) from a fit to a 38 ks *XMM-Newton*/EPIC spectrum, is not confirmed by a deeper *Suzaku* observation and in fact may be 30



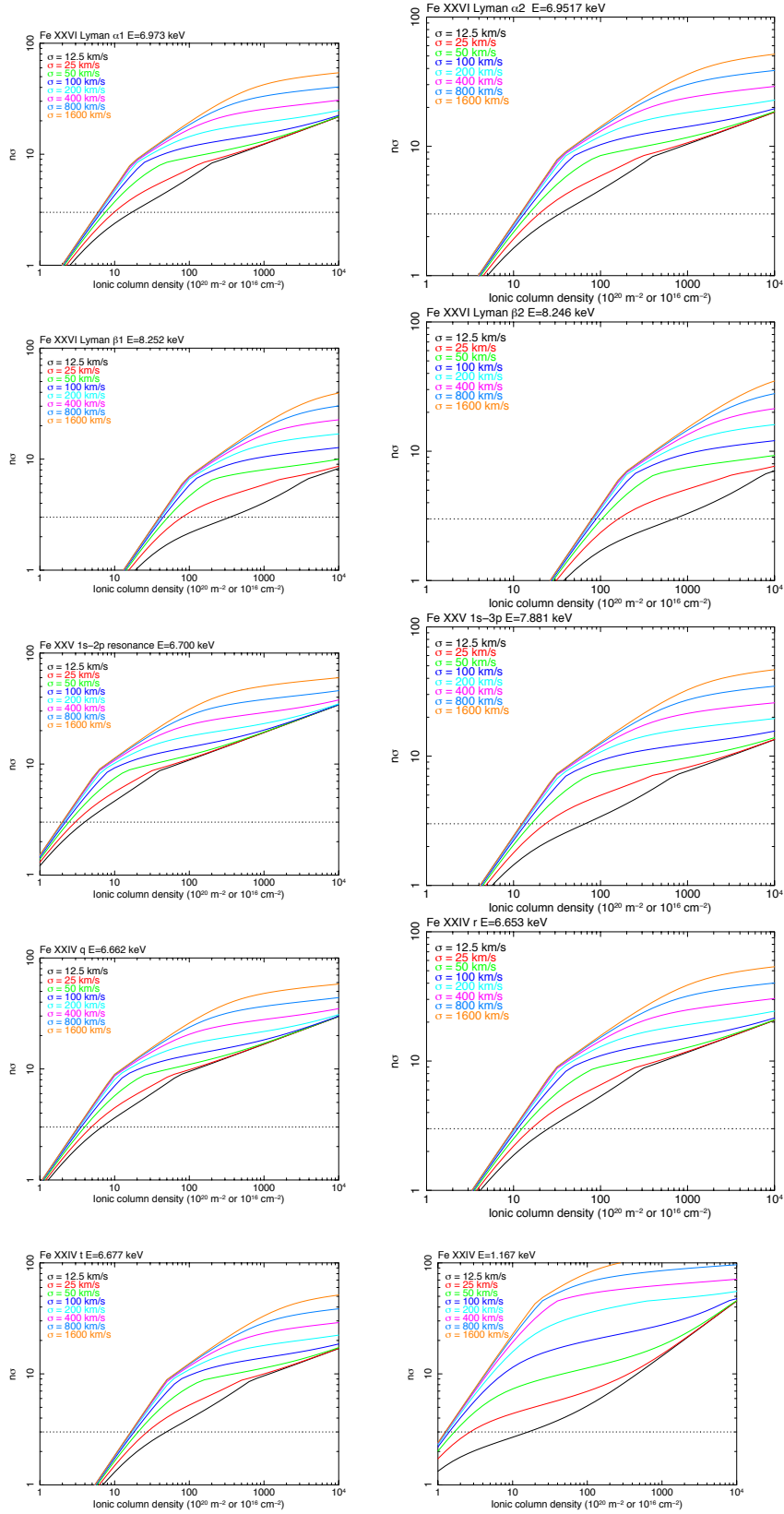


**Figure 2:** Detection significances ( $n\sigma$  is  $S/N$ ) for a 100 ks exposure on a typical bright AGN with parameters as described in the text, for different Gaussian velocity broadening as indicated. The dotted horizontal lines indicate the  $3\sigma$  detection limits.

times lower (Bianchi et al., 2010). Also, a yet unpublished 120 ks *Chandra* HETG spectrum shows no signs of strong absorption lines.

In the next sections we make a few dedicated simulations for *ASTRO-H* for some of the most promising sources.

### 1.3.1 NGC 4151

We simulated the spectrum of NGC 4151 using the same flux condition of the 2002 HETG spectrum (Kraemer et al., 2005). We used their absorber model (adopting the *xabs* model fo SPEX for the absorbers) and added two *slab* components for the higher ionization gas. See Table 1 for the parameters and Figure 3 for the simulated spectrum.

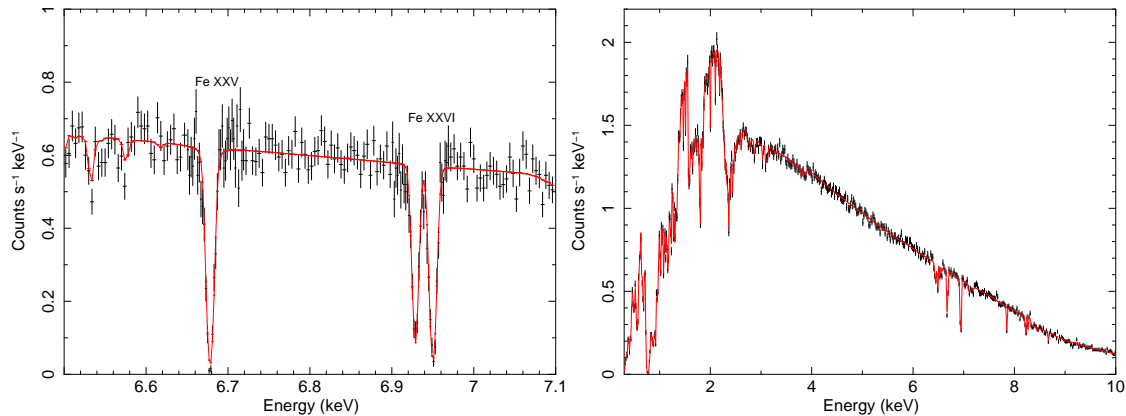


**Figure 3:** Simulated spectrum for NGC 4151 for 100 ks exposure time.

**Table 1:** Simulated parameters for NGC 4151. Column densities in  $\text{cm}^{-2}$ .

Simulated parameters	
Exposure	100 ks
Flux (2–10 keV)	$1.9 \times 10^{-10}$ cgs
xabs 1	$\log N_H = 22.5$ ; $\log \xi = 2.55$
xabs 2	$\log N_H = 22.46$ ; $\log \xi = 1.23$
xabs 3	$\log N_H = 20.8$ ; $\log \xi = -0.17$
xabs 4	$\log N_H = 21.6$ ; $\log \xi = 0.42$
xabs 5	$\log N_H = 20.8$ ; $\log \xi = -0.09$
Fitted parameters	
slab 1	$\log N_{\text{Fe XXV}} = 17.94 \pm 0.02$
slab 2	$\log N_{\text{Fe XXVI}} = 17.88 \pm 0.04$

Note that the flux during the 2002 *Chandra* HETG observation that we used as a template is rather high. It is in most cases a factor of 2 dimmer, on average. Hence, a twice as long exposure time (200 ks) would be needed for a typical flux state.

### 1.3.2 NGC 3783

The spectrum of NGC 3783 was simulated as follows (Figure 4). The continuum parameters were adjusted in the way described earlier in this white paper with a 2–10 keV flux of  $5.2 \times 10^{-11}$  cgs. The Fe  $K\alpha$  emission line

was modelled with a single Gaussian whose parameters match the average result of the Yaqoob et al. (2005) analysis ( $E_0 = 6.397$  keV,  $\text{FWHM} = 1700$  km s $^{-1}$ ). The model includes 3 lower  $\xi$  components, as described in Netzer et al. (2003). For the simulation we added two more components with corresponding ionization parameters of 3.7 and 4.1, respectively. Their column densities are scaled from the highest value reported in Netzer et al. (2003) using  $\xi^{0.2}$ . For an exposure time of 100 ks we can determine the Fe XXV and Fe XXVI columns with an accuracy of 17% and 19%, respectively. The optical depth of the strongest 1s–2p transitions at line center is 15.7 for Fe XXV, and 5.0 for Fe XXVI, and so the lines have a strong saturation. This means that even if the column density is much lower, the lines still can be detected easily.

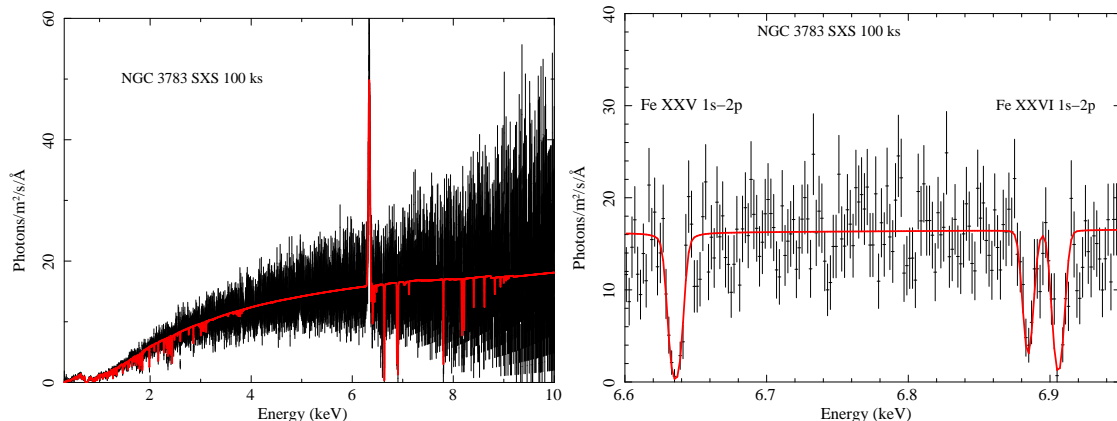


**Figure 4:** Simulated spectrum for NGC 3783 for 100 ks exposure time. The left panel shows the full spectrum; due to the strong compression of this high resolution spectrum along the horizontal axis, the error bars look larger than they are: the right panel shows a blow-up near the iron lines and demonstrates the true power of the SXS.

### 1.3.3 NGC 5548

We re-analysed the 340 ks *Chandra* LETG data of the Seyfert 1 galaxy NGC 5548 using the radiation transfer code with the latest atomic data (CLOUDY v10; Ferland 2002) and the software package optimized for high-resolution X-ray spectroscopy (SPEX v2.04; Kaastra et al. 1996). Following the previous work (Steenbrugge et al., 2005), we fitted the spectrum with a model consisting of a power-law plus a black body continuum with ionized absorbers. We found that at least four distinct absorbers with different ionization degrees are required to explain the absorption features. Steenbrugge et al. (2005) showed that the spectrum represents five absorption components. We derived the ionization parameter  $\xi$ , the column density and outflowing velocity for each component. Tables 2 and 3 show a summary of the fitting parameters. The details will be described in Seta et al. in prep.

**Table 2:** Summary of continuum parameters

Parameter	
power law: norm ( $10^{52}$ ph/s/keV at 1 keV)	$0.56 \pm 0.01$
power law: $\Gamma$	$1.72 \pm 0.02$
modified blackbody: area $\times$ density ( $10^{33}$ cm $^{0.5}$ )	$2.21 \pm 0.16$
modified blackbody: $T$ (in eV)	$125 \pm 4$

We simulated the spectrum of NGC 5548 based on these parameters. We added two components with Fe XXV and Fe XXVI columns. When the values of the Fe XXV and Fe XXVI columns are about  $1.5 \times 10^{21}$  cm $^{-2}$ , we found that we can detect the Fe XXV column with an integration time of 2 Ms at  $3\sigma$ . On the

**Table 3:** Summary of absorption parameters

Comp.	$\log \xi$	$N_{\text{H}}$ ( $10^{21} \text{ cm}^{-2}$ )	RMS velocity (km/s)	Average velocity (km/s)
a	$1.14 \pm 0.05$	$0.60 \pm 0.07$	$95.3^{+13.1}_{-17.8}$	$-433.5^{+24.3}_{-28.4}$
b	$1.99^{+0.03}_{-0.05}$	$0.86^{+0.17}_{-0.15}$	$44.4^{+26.1}_{-14.6}$	$-276.9^{+51.3}_{-47.7}$
c	$2.34 \pm 0.03$	$3.77^{+0.80}_{-0.68}$	$33.3^{+6.9}_{-6.1}$	$-967.9^{+26.6}_{-25.9}$
d	$3.07 \pm 0.04$	$7.19^{+2.50}_{-1.56}$	$88.8^{+37.1}_{-31.7}$	$-479.6^{+74.7}_{-62.1}$

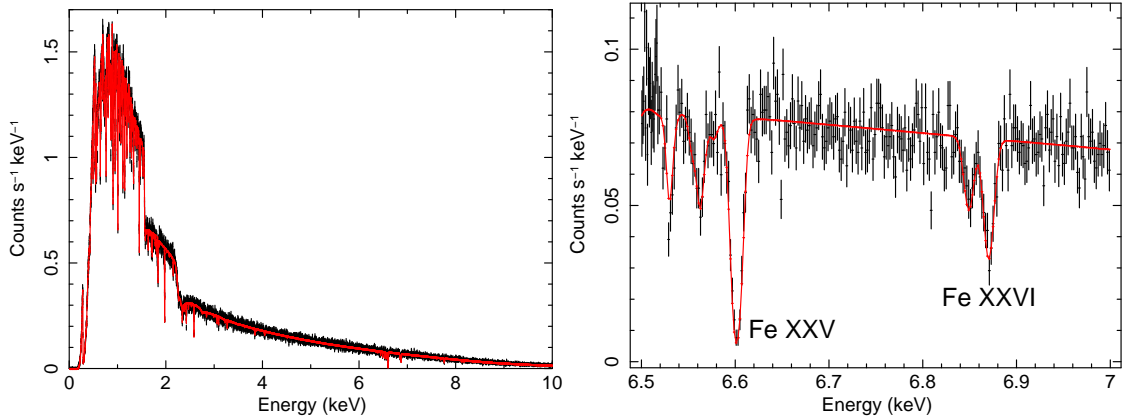


**Figure 5:** Simulated spectrum for NGC 5548 for 700 ks exposure time.

other hand, the Fe XXVI column is undetectable. When the values of the Fe XXV and Fe XXVI columns are ten times larger than this, we found that we can detect the Fe XXV and Fe XXVI columns with an integration time of 700 ks at  $3\sigma$ . The left panel of Figure 5 shows the simulated spectrum of a 700 ks exposure time. The right panel of Figure 5 shows a close-up view of the Fe XXV and Fe XXVI absorption lines.

### 1.3.4 NGC 3516

We simulated the spectrum of NGC 3516 based on the *XMM-Newton* EPIC observation published by (Turner et al., 2008). The exposure time of 200 ks was chosen to detect the ionic column density of Fe XXV at least at  $5\sigma$  significance. Note the saturation of the 1s–2p lines (Fe XXV and Fe XXVI, see Figure 6). The resulting best-fit column densities are  $(4.8 \pm 0.8) \times 10^{17} \text{ cm}^{-2}$  and  $(2.6 \pm 0.4) \times 10^{18} \text{ cm}^{-2}$  for Fe XXV and Fe XXVI, respectively.

The model consists of 4 warm absorbers, but only two have a visible effect in the iron region, see Figure 6. They are modelled with the *xabs* model of SPEX. The components have hydrogen column densities (in units of  $10^{16} \text{ cm}^{-2}$ ) of 24, 5, 2020 and 2620, respectively, with  $\log \xi$ -values of  $-2.43$ ,  $0.25$ ,  $2.19$  and  $4.31$ . Components 1 and 2 have zero outflow velocity, while component 3 has an outflow velocity of  $-1600 \text{ km s}^{-1}$  and component 4 of  $-1000 \text{ km s}^{-1}$ . Component 3 has a covering factor of 0.45, while all other components have covering factor unity. The continuum is a simple power-law with photon index 1.9 and 2–10 keV flux of  $5.4 \times 10^{-11} \text{ cgs}$ .

Note that the source is highly variable in the 0.5–2 keV band (orders of magnitude), but not extremely variable in the medium band (2–10 keV, max variation a factor of 5). We simulated a relatively high state, recorded in 2006. The parameters taken from *XMM-Newton* EPIC data analysis (Turner et al., 2008).

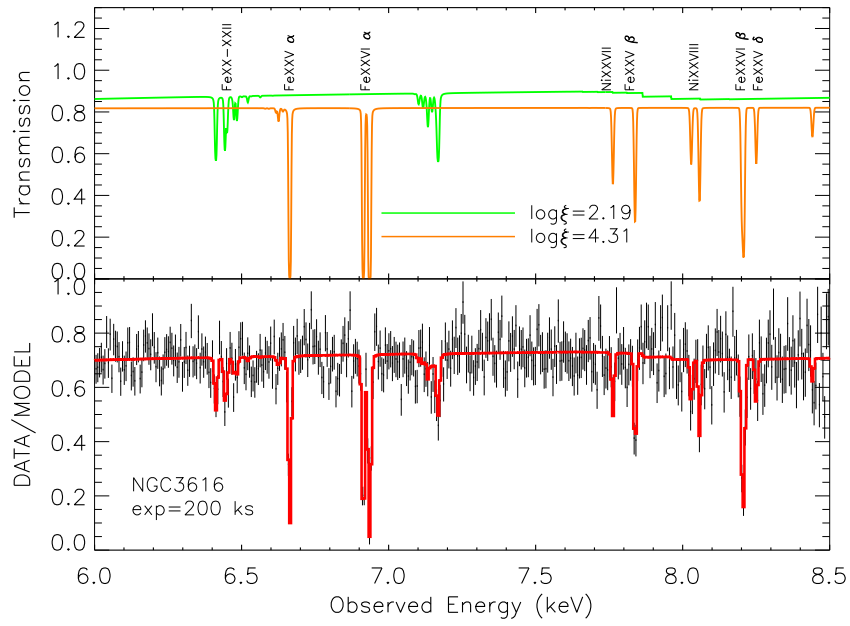


**Figure 6:** Simulated spectrum for NGC 3516 for 200 ks exposure time.

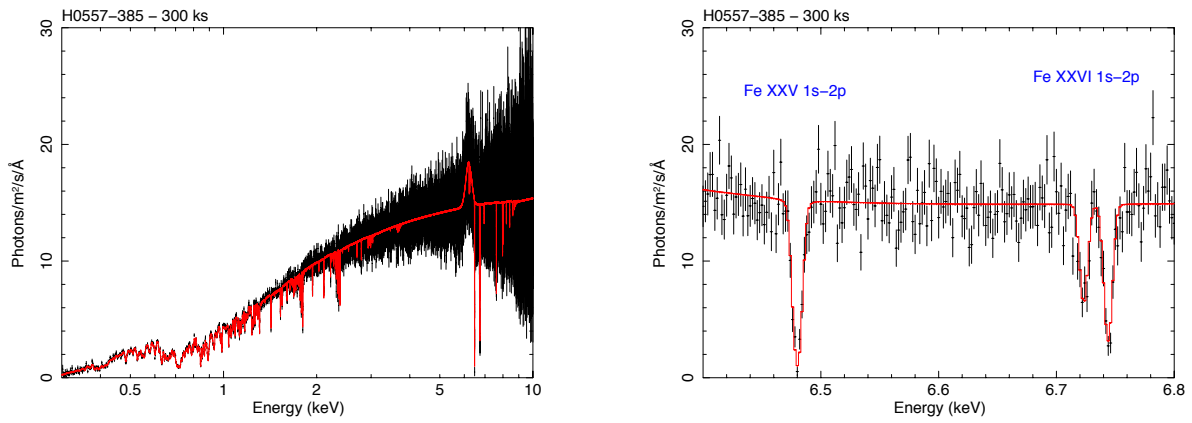


**Figure 7:** Simulated spectrum for H 0557-385 for 300 ks exposure time. See also the remark at Figure 4.

### 1.3.5 H 0557-385

We simulated the spectrum of H 0557-385 based on the *XMM-Newton* observation published by Ashton et al. (2006). The model includes two lower- $\xi$  components observed with *XMM-Newton*. We add two components with Fe XXV and Fe XXVI columns of  $4$  and  $5 \times 10^{21} \text{ cm}^{-2}$ , respectively, and found that for an integration time of 200 ks we can measure the Fe XXV and Fe XXVI columns with 20 and 38% accuracy, respectively. To get Fe XXVI to the 20% level would require 500 ks exposure time. An exposure time of 300 ks appears to be a good compromise and has been used for the simulation shown in Figure 7. The optical depth of the strongest 1s–2p lines at line center is 6.2 for Fe XXV and 2.6 for Fe XXVI.

We note here that H 0557-385 is usually in a bright state corresponding to our simulated spectrum. However, it has been observed once in a ten times dimmer state with very interesting Fe-K emission line properties (Longinotti et al., 2009) ascribed to intervening line-of-sight clouds.

## 1.4 Beyond Feasibility

Time variability of the outflow can be used to determine or constrain the absolute location of the outflowing gas, by measuring delays of the ionisation state with respect to changes in the ionising continuum. This delay is essentially the recombination time scale, that scales inverse proportional to the density. Most observations of outflows with *ASTRO-H* will likely be long, 100 ks or more, which means that the total duration of the observation will be a few days. Less massive AGN will show significant continuum variations during the observation and therefore allow to constrain recombination time scales at the day time scale. For more massive AGN, or for less massive AGN for longer time scales, a second observation separated by weeks or half a year from the first one will allow the same study but for longer time scales.

Further, SXS is most sensitive to the highest ionised gas. In order to derive the full absorption measure distribution, simultaneous observations with the *Chandra* or *XMM-Newton* gratings will allow for such a complete picture. In this respect in particular the *Chandra* LETG and *XMM-Newton* RGS are most useful, because they are sensitive to the softest X-rays. The use of *XMM-Newton* has the additional benefit of yielding simultaneously the UV continuum through data from the Optical Monitor. This UV continuum is needed for accurate photoionisation calculations.

Finally, depending on the properties of the outflow, it may be possible to measure the covering factor of the X-ray source by the outflow, therefore providing a direct estimate of its size. This can be achieved by comparing the intensity of two or more lines from the same ion, for instance the  $\text{Ly}\alpha$  doublet of Fe XXVI.

## 2 Ultra Fast Outflows

### 2.1 Background and Previous Studies

The advent of the high throughput CCDs on board *XMM-Newton*, *Chandra* and later *Suzaku* brought also additional, somewhat unexpected discoveries in the field of X-ray spectroscopy and in particular regarding AGN outflows.

For instance, Chartas et al. (2002, 2003) reported the first evidences for BAL quasar type of outflows in the *Chandra* and *XMM-Newton* X-ray spectra of the gravitationally lensed, high redshift ( $z \geq 2$ ) quasars APM 08279+5255 and PG 1115+080 through the detection of absorption lines at rest-frame energies  $E > 7 \text{ keV}$ . Meanwhile, Pounds et al. (2003) reported the detection with *XMM-Newton* of similar absorption lines also in the local ( $z = 0.08$ ) quasar PG 1211+143, which then became the archetype for such type of outflows. If identified with Fe XXV/XXVI absorption lines, these features suggest the presence of previously unknown highly ionized zones of circumnuclear absorbing material with large column densities and blue-shifted velocities reaching mildly-relativistic values of  $\sim 0.1\text{--}0.3c$ , which are possibly directly connected with accretion disk winds/outflows.

Indeed, detailed theoretical studies of accretion disk winds in AGNs show that the inner parts of the outflow can be highly ionized by the intense nuclear radiation and, in principle, can easily reach mildly-relativistic

velocities (e.g. King & Pounds, 2003; Ohsuga et al., 2009; King, 2010; Fukumura et al., 2010). Therefore, when the line of sight to the observer intercepts the flow, considerable absorption features from highly ionized species can be imprinted in the X-ray spectrum in the form of blue-shifted Fe XXV/XXVI K-shell absorption lines at rest-frame energies greater than  $\sim 7$  keV.

Following these first seminal cases, several papers reporting the detection of similar blue-shifted absorption lines in a number of low-redshift Seyfert galaxies and quasars appeared in the literature as well, although the claimed features often had only a limited statistical significance of  $\approx 3\text{--}4\sigma$ . In fact, an important drawback regarding these features is due to the fact that for low-redshift sources (representing the majority of the cases) they appear at energies  $E > 7$  keV, a region of the spectrum where the instrumental resolution and signal-to-noise of the present X-ray instruments are very limited. Moreover, due to its high ionization, this material is hard to observe in soft X-ray spectra because all the elements lighter than Fe are almost completely stripped of their electrons and this may be one of the reasons why it was not reported previously.

Nevertheless, the first systematic and comprehensive search for blue-shifted Fe K absorption lines at  $E \geq 7$  keV in a large sample of 42 local ( $z \leq 0.1$ ) Seyferts observed with *XMM-Newton* was performed by Tombesi et al. (2010a). They estimated the absorption line parameters carrying out a uniform modeling of all datasets and calculated the detection significance making use of both the F-test and extensive Monte Carlo simulations. In order to mark an initial distinction with the more typical warm absorbers, which usually show maximum velocities lower than a few  $1000 \text{ km s}^{-1}$ , Tombesi et al. (2010a) also defined ultra-fast outflows (UFOs) as those highly ionized absorbers detected essentially through Fe XXV and/or Fe XXVI lines with a blue-shifted velocity higher than  $10000 \text{ km s}^{-1}$  ( $\approx 0.03c$ ). The majority of the detected lines are consistent with UFOs and their observed fraction is  $\sim 30\text{--}40\%$ , indicating that UFOs could possibly represent a common phenomenon taking place in these radio-quiet AGNs. Although hampered by the limited CCD sensitivity, the data indicate possible variability of some of the line equivalent widths and velocity shifts among different observations of the same sources, even on time-scales shorter than days, possibly indicating compact absorbers. Noteworthy, these results have been confirmed also by an independent analysis of a large sample of AGNs performed by Gofford et al. (2012) using broad-band *Suzaku* data.

Despite the significant uncertainties due to the limited CCD sensitivity and energy resolution, photo-ionization modeling of the blue-shifted Fe K absorption lines associated with UFOs has been performed using codes such as *Xstar* (e.g., Tombesi et al., 2011; Gofford et al., 2012). As anticipated, the outflow velocity distribution is found to be mildly-relativistic, in the range  $\approx 0.03\text{--}0.3c$  ( $\approx 10000\text{--}100000 \text{ km s}^{-1}$ ), with mean value of  $\approx 0.1c$ . The ionization is in the range  $\log \xi \approx 3\text{--}6$  and the column densities are in the interval  $N_{\text{H}} \approx 10^{22}\text{--}10^{24} \text{ cm}^{-2}$ . Some of these models will be used as templates to carry out the realistic *ASTRO-H* calorimeter simulations reported in the subsequent sections.

Several papers have been published attempting to estimate the location and energetics of these UFOs. However, due to the large uncertainties, they have been able to place only order of magnitude lower/upper limits. For instance, Tombesi et al. (2012) performed a uniform investigation of these parameters in a large sample of Seyferts galaxies. On average, the UFOs seem to be observed at sub-pc distances from the central supermassive black hole, corresponding to  $\approx 10^2\text{--}10^4$  Schwarzschild radii. Their mass outflow rates are probably in the range between  $\approx 0.01\text{--}1 M_{\odot} \text{ yr}^{-1}$  and, given their high velocity, their associated mechanical power can easily reach very high values of  $\dot{E}_K \approx 10^{42}\text{--}10^{44} \text{ erg s}^{-1}$ , which might be even comparable to that of some of the jets in radio galaxies. In particular, these values are systematically larger than  $\sim 0.5\%$  of the bolometric luminosity, which is the minimum ratio required by numerical simulations of feedback induced by AGN winds/outflows (e.g., Hopkins & Elvis, 2010).

Therefore, overall, these results point to the conclusion that such UFOs might indeed have the possibility to bring outward a significant amount of mass and energy from the central regions of AGNs, which can then have an important influence on the surrounding environment (e.g., Cappi, 2006). Feedback from AGNs is expected to have a significant role in the evolution of the host galaxies, such as the enrichment of the ISM or the quenching of star formation, and could also contribute to the establishment of some fundamental relations, such as the  $M_{\text{BH}}\text{--}\sigma$ . The ejection of a significant amount of mass from the central regions of AGNs could also inhibit the growth of supermassive black holes, potentially affecting their evolution. Therefore, the UFOs might

well represent the long sought-after agent mediating the “quasar mode” galaxy feedback.

The UFOs, and some of the other more “normal” AGN outflows (e.g., Crenshaw & Kraemer, 2012), might actually provide a feedback impact comparable or even greater than that from jets. In fact, the UFOs are likely more massive than jets. They are mildly-relativistic and have somewhat wide angles, therefore possibly exerting a higher impact on the surrounding host galaxy environment compared to the highly collimated relativistic jets, which might actually drill out of the galaxy and have a dominant effect only in the outside. UFOs are energetic, with a mechanical power possibly comparable to that of jets. Moreover, evidences for UFOs have been found in at least  $\sim 30\text{--}40\%$  of the local radio-quiet AGNs and may possibly have a more widespread feedback influence with respect to the less common radio-loud sources with powerful jets.

In this respect, it is important to note that evidences for UFOs have been reported in some radio-loud AGNs as well (Tombesi et al., 2010b; Gofford et al., 2012) and therefore their feedback effect might actually be concomitant with that from jets. This opens also a new line of investigation that can help to shed light on the intricate connection between the accretion disk and the formation of jets and outflows, similarly to what has been reported for the radio galaxies 3C 111 and 3C 120 (Chatterjee et al., 2009, 2011) and the micro-quasar GRS 19151+105 (Neilsen & Lee, 2009). Comparing the mechanical power of winds and jets from stellar mass to supermassive black holes, King et al. (2013) recently suggested that the characteristics of UFOs tend to resemble those of jets more than winds, indicating that we may be observing a transition regime in which winds become jets. This, as well as other evidences, may open the unexpected possibility to effectively study jet related events through X-ray absorption line spectroscopy.

We note that some of the AGNs in which evidences for UFOs have been reported also simultaneously show the more “normal” outflows in the soft X-rays. This rises the issue of what is, if any, the connection between these two type of ionized absorbers. One of the first attempts to find an answer to this question was reported very recently by Tombesi et al. (2013), who performed a comparison of the characteristics of the UFOs and the warm absorbers in a sample Seyfert 1 galaxies observed with *XMM-Newton* and *Chandra*. For the first time, they claim the existence of correlations between the different parameters, indicating that the closer the absorber is to the central black hole, the higher the ionization, column density, outflow velocity and consequently the mechanical power. This suggests that these absorbers could actually be unified as parts of a single, large-scale stratified outflow observed at different locations along the line of sight, from the vicinity of the central supermassive black hole up to the outskirts of the host galaxy. The actual acceleration mechanism(s) of these outflows are still unknown and this represents one of the main challenges posed to both observation and theory. For instance, Tombesi et al. (2013) suggests that the observations are consistent with a combination of radiation pressure through Compton scattering (e.g., King & Pounds, 2003) and/or MHD processes (e.g., Fukumura et al., 2010), the latter being in agreement with the wind-jet connection suggested by King et al. (2013).

## 2.2 Prospects & Strategy

In the previous section we described a series of amazing scientific implications and the broad impact on the physics of AGNs and galaxy evolution brought by the discovery of UFOs. However, it is important to note that there is a fundamental drawback in the study of UFOs through blue-shifted Fe XXV-XXVI absorption lines at  $E > 7$  keV with current CCD instruments. Often, just one absorption line is detectable and the great majority of the detections are weak, in the range between  $\sim 3\text{--}4\sigma$ . Since the initial claims of detections, this raised strong debates and criticisms in the community and, despite the improvements in recent years, the issue has not been fully solved yet and there are even scepticisms about the actual existence of these UFOs. In the next sections we will show that the unprecedented energy resolution and sensitivity in the crucial  $E = 4\text{--}10$  keV band provided by the *ASTRO-H* calorimeter will allow a fundamental breakthrough in this field and the definitive solution of this problem.

One major point will be not just the increased detection significance of each single weak absorption line, but the possibility to simultaneously detect more than one line from the same photo-ionized absorber. From a previous *XMM-Newton* sample study of blue-shifted Fe XXV-XXVI absorption lines, Tombesi et al. (2011) reported that in 19 cases the lines were consistent with UFOs and for each of these only a single significant line



was detected. Using the photo-ionization code *Xstar*, they identified 9 lines with Fe XXVI, 4 with Fe XXV and for 6 of them the identification was degenerate (at the 90% level) between Fe XXV or Fe XXVI. Instead, Gofford et al. (2012) using *Suzaku* reported lines consistent with UFOs in 12 cases, 6 of which were single and identified with Fe XXVI, 3 single but degenerate between Fe XXV or Fe XXVI, 2 blended and 1 double identified with both Fe XXV and Fe XXVI together. With *ASTRO-H*, we expect the number of detected double lines to significantly increase, drastically improving the significance of the observed UFOs. Additionally, higher order transitions of Fe XXV-XXVI and absorption lines from lighter elements as well (such as S, Si, Ca, Ar) could be possibly detected by *ASTRO-H*.

For instance, if we detect two lines each with null hypothesis significances  $p_1$  and  $p_2$  of  $\sim 3\sigma$  (corresponding to  $\sim 99.9\%$  chance probability), their combined detection level  $P \approx p_1 \times p_2$  effectively increases to  $\sim 5\sigma$  ( $\sim 99.9999\%$  chance probability). Thus, the simultaneous detection of multiple lines from Fe XXV and/or Fe XXVI will tremendously boost the detection significance of the associated UFOs and will drastically lower the minimum sensible column densities (even down to  $N_H \sim 10^{20} \text{ cm}^{-2}$ ). Considering the full  $E \approx 0.5\text{--}10 \text{ keV}$  band, *ASTRO-H* will allow also to simultaneously detect different absorption components, from the soft X-rays to the hard X-rays, and dramatically expand the observed range in ionization, column density and outflow velocity. The expected detection of several lines in the Fe K band will potentially provide a breakthrough comparable to that brought to the warm absorber studies by the advent of the grating spectrometers on board *Chandra* and *XMM-Newton*. Therefore, it is likely that with *ASTRO-H* the UFO could actually become the new “normal” type of outflows.

Only a handful of the absorption lines detected with the CCDs have been resolved. In general, their velocity broadening ( $\sigma_v$ ) is expected to be in the range between  $\sim 1\,000 \text{ km/s}$  up to  $\sim 5\,000 \text{ km/s}$ . The calorimeter will allow to resolve all these lines and to even study the profile for the broadest ones, drastically decreasing the uncertainties on the column density and possibly helping to test the different profiles expected from radiation or MHD acceleration mechanisms (e.g., Fukumura et al., 2010). Due to the limited energy resolution of the present CCDs, in many cases the lines appear also blended together and their identification can be degenerate between Fe XXV and/or Fe XXVI. The detection of more lines with the calorimeter will allow to better discriminate between different ionization levels.

Finally, we note that previous CCD observations suggested that the blue-shifted Fe XXV-XXVI absorption lines may show variability in both EW and velocity shift even on time scales shorter than days, in accordance with the idea that the UFOs are ejected from the inner accretion disk close to the black hole and that they represent the most dynamically important outflow component. Their variability could be due to a response to changes in the source luminosity or could be intrinsic, possibly depending also on their unknown ejection duty cycle. In general, studies of large samples find a detection frequency of  $\sim 30\%$  (Tombesi et al., 2010a; Gofford et al., 2012). Therefore, in order to take into account the possibility of detection/non-detection due to their intermittent nature, our preferred strategy should be on observing more sources or one source multiple times. For instance, from the observation of 10 sources we expect to detect UFOs in at least  $\sim 3$  of them or, equivalently, we expect at least one secure detection out of  $\sim 3$  observations. This point is very important because it represents another of the main criticisms on the actual existence of UFOs, which says that the “spurious” detection of weak lines in different observations could just indicate random noise.

In the next sections we will better quantify these claims, we will derive some exposure time estimates for a sample of possible candidate sources and we will show some realistic simulated spectra.

### 2.3 Targets & Feasibility

We selected the targets from the local ( $z < 0.1$ ) AGNs with detected UFOs reported in Tombesi et al. (2010a,b) and Gofford et al. (2012). The equivalent widths of the Fe XXV and/or Fe XXVI absorption lines relative to the UFOs are in the range from  $\approx 15 \text{ eV}$  up to  $\approx 100 \text{ eV}$ , with mean and median values of  $\approx 50 \text{ eV}$  and  $\approx 30 \text{ eV}$ , respectively. The average blue-shifted velocity of these lines is  $\approx 0.1c$ , which corresponds to an observed energy of  $E \approx 8 \text{ keV}$ . Therefore, we consider the most conservative case assuming only one line at  $8 \text{ keV}$  (where the effective area is  $\approx 200 \text{ cm}^{-2}$ ) with the minimum observed equivalent width of  $\text{EW} = 15 \text{ eV}$  and for each source

we consider the minimum 4–10 keV flux level among the relative observations. Then, we use equation 9 to calculate the minimum exposure time required to reach a detection confidence level of  $5\sigma$ . The approximate exposure times for all the candidate sources were calculated. Due to the fast decrease in effective area, to detect the same line at  $\sim 9$  keV, corresponding to a velocity shift of  $\sim 0.2c$ , it would require an increase of  $\sim 60\%$  in exposure. We find that for sources with 4–10 keV flux  $\geq 1 \times 10^{-11}$  erg s $^{-1}$  cm $^{-2}$  it will be even possible to also study very short time-scale variability on  $\sim 20$  ks time-scales. In the next sections we show a few dedicated simulations for *ASTRO-H* relative to some of the most promising sources.

### 2.3.1 Mrk 509

We performed a 100 ks realistic *ASTRO-H* calorimeter simulation of the Seyfert 1 galaxy Mrk 509, which has been claimed to show UFOs in some of its *XMM-Newton* observations. We assume the same spectrum as of the *XMM-Newton* observation of April 2006 in which the detection of a weak blue-shifted absorption line with  $EW \approx 20$  eV at the rest-frame energy of  $\approx 8.5$  keV was reported (Cappi et al., 2009; Tombesi et al., 2010a). Due to the limited CCD resolution and sensitivity, it was not possible to discriminate between Fe XXV or Fe XXVI and a fit with an *Xstar* table with turbulent velocity of 1,000 km s $^{-1}$  gave two relative solutions with average outflow velocity of  $\sim 0.2c$ . We focus in the E=4–10 keV band and assume the Fe XXVI model of Tombesi et al. (2011). The simulated spectrum is shown in Figure 8. Imposing a fit with the Fe XXV model, we find that it is rejected with a  $\Delta\chi^2 \sim 33$ , which corresponds to a  $\sim 5\sigma$  level. Therefore, *ASTRO-H* will indeed be able to clearly discriminate between the two possible solutions. Instead, fitting with the Fe XXVI model, we find an improvement of  $\Delta\chi^2 \sim 80$ , indicating that the UFO will be detectable at  $\gg 5\sigma$  (compared only to a  $\Delta\chi^2 \sim 15$  of *XMM-Newton*).

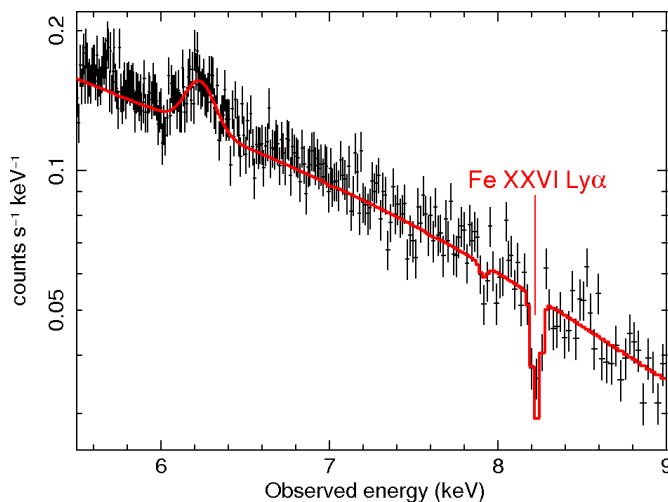


**Figure 8:** Simulated 100 ks *ASTRO-H* calorimeter spectrum of Mrk 509 using the *XMM-Newton* observation of April 2006 as baseline. The highly ionized UFO has a velocity  $\approx 0.2c$ . The dataset has been grouped to a S/N of 10 for each energy bin.

### 2.3.2 3C 111

We performed a 100 ks realistic *ASTRO-H* calorimeter simulation of the broad-line radio galaxy 3C 111 based on the 100 ks *Suzaku* XIS spectrum taken in 2008. We focused only in the E=4–10 keV band. Blue-shifted Fe K absorption lines were detected in this spectrum by Tombesi et al. (2010b) and Gofford et al. (2012), indicating that this is one of the few radio-loud AGN showing UFOs to date. Interestingly, this source shows also a

powerful, time variable relativistic radio jet and was detected in the  $\gamma$ -rays with the Fermi satellite. Therefore, the study of its UFO has important implications for the investigation of the possible connection between the disk, the jet and outflows and their feedback on the host galaxy.

We assume the best-fit model of Tombesi et al. (2010b), which is composed of a Galactic absorbed power-law continuum with  $\Gamma \simeq 1.5$ , a neutral Fe  $K\alpha$  emission line and an *Xstar* component with turbulent velocity of  $1000 \text{ km s}^{-1}$ , column density  $N_H \simeq 10^{23} \text{ cm}^{-2}$ , high ionization  $\log \xi \simeq 5$  and outflow velocity of  $v_{out} \simeq 0.04c$ . We note that during this observation the source was caught in an historical flux minimum of  $\sim 1 \times 10^{-11} \text{ erg s}^{-1} \text{ cm}^{-2}$ . From Figure 9 we can clearly note the huge improvement in the detection of the blue-shifted absorption lines between the 100 ks combined *Suzaku* XIS 0+XIS 3 spectrum on the left and the simulated 100 ks *ASTRO-H* calorimeter on the right. Many more absorption lines are clearly observable with the calorimeter. The fit improvement given by the addition of the *Xstar* absorption component in the calorimeter spectrum is enormous,  $\Delta\chi^2 = 280$  for three free parameters, instead of the mere  $\Delta\chi^2 \simeq 22$  of the *Suzaku* observation. This would allow to clear any doubts about the real detection of the UFO, which will be detectable at a  $\sim 20\sigma$  significance level. The estimates of the absorber parameters will be significantly improved as well, for instance the column density will be estimated with  $\sim 15\%$  errors (presently only lower limit with *Suzaku*), the ionization with  $2\%$  and the velocity with  $<1\%$  (both  $\sim 10\%$  with *Suzaku*). For the most intense absorption line, the Fe XXVI  $\text{Ly}\alpha$ , the centroid energy will be constrained with  $0.05\%$  errors (10 times better than *Suzaku*), the line will be resolved with  $<10\%$  errors (presently not resolved *Suzaku*), allowing to estimate the velocity broadening, and the EW will be estimated with  $5\%$  error.

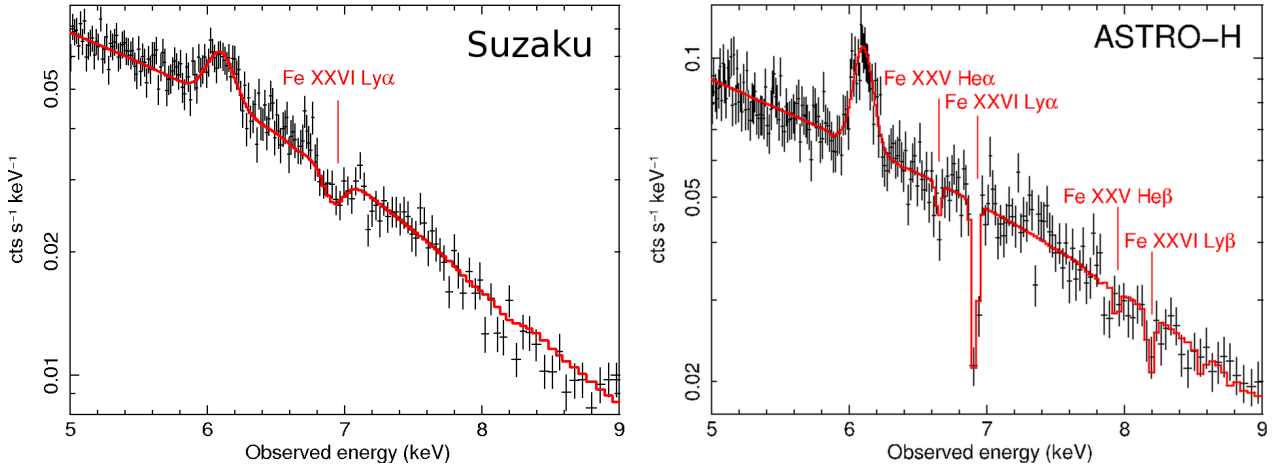


**Figure 9:** Spectrum of the radio galaxy 3C 111 showing a UFO with velocity  $\simeq 0.04c$ . *Left panel:* real 100 ks combined *Suzaku* XIS 0+XIS 3 spectrum obtained in 2008. *Right panel:* simulated 100 ks *ASTRO-H* calorimeter spectrum. Both datasets have been grouped to a S/N of 10 for each energy bin.

### 2.3.3 PG 1211+143

PG 1211+143 ( $z = 0.0809$ ) is the quasar in which Pounds et al. (2003) first reported the detection of highly ionized blueshifted iron absorption features. A subsequent analysis with detailed photoionization modeling by Tombesi et al. (2011), these features are well reproduced by an highly ionized ( $\log \xi = 2.87$ ) outflowing ( $v_{out} = 0.15c$ ) gas along the line of sight (with column density of about  $10^{23} \text{ cm}^{-2}$ ).

Here, we present the results of the SXS calorimeter simulation of PG 1211+143 based on the *XMM-Newton* observation in 2001. We used the redistribution matrix function (RMF) with 5 eV resolution, which is the current best-estimated version (ah\_sxs\_5ev\_basefit\_20100712.rmf), and the ancillary response file (ARF) for the point source (sxt-s\_120210\_ts02um\_of\_intallpx1.arf). The model assumed is based on Tombesi et al. (2011). Errors are quoted at 68% confidence, for one parameter of interest.

Figure 10 shows the simulated spectrum in the 5–9 keV energy band for 100 ks exposure. The broad and

deep trough is clearly seen around 7 keV. In order to estimate the significance of the absorption feature, we applied a single power-law and a negative Gaussian model to the data. The line center energy (source rest frame) and the broadening are determined to be  $E = 7.65 \pm 0.03$  keV and  $\sigma = 156_{-23}^{+33}$  eV, respectively. The equivalent width derived is  $-186_{-67}^{+58}$  eV. In order to investigate the absorption feature in more detail, we applied a power-law absorbed by an ionized absorber calculated via XSTAR photoionization code (Kallman & Bautista 2001). We assumed the turbulent velocity to be  $5000 \text{ km s}^{-1}$ . The inclusion of the XSTAR model improves the fit significantly ( $\Delta\chi^2 = 52$  for three additional parameters). We are able to strictly constrain the outflow velocity  $v_{\text{out}}$  to be  $0.154_{-0.002}^{+0.001}c$ . The column density and ionization parameter are determined to be  $N_{\text{H}} = 1.0_{-0.2}^{+0.3} \times 10^{23} \text{ cm}^{-2}$  and  $\log \xi = 2.9_{-0.3}^{+0.2}$ , respectively.

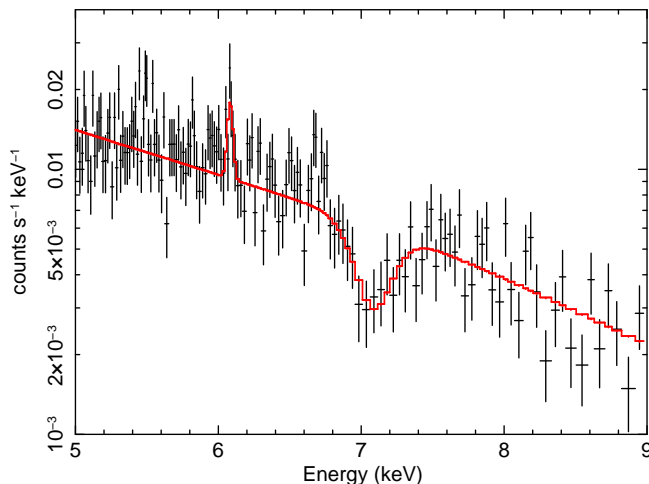


**Figure 10:** Simulated spectrum of PG 1211+143 for 100 ks observation. The absorption feature around 7 keV is due to Fe XXV.

### 3 Comparison with numerical models

#### 3.1 Background and Previous Studies

Most theoretical modelling of AGN winds as it relates to X-ray properties has been directed toward the question of how the winds are created and what their structure is. This has implications for understanding the effects of winds on the UV region of the spectrum, and therefore on larger questions about AGN: their mass budget, their black hole masses, and their evolutionary state. In principle, construction of a model for testing against X-ray data should consist of: (i) begin with a physical model of an AGN, i.e. the dynamics of the gas affecting the observed spectrum, followed by (ii) a calculation or a realization of the dynamical model, and then performing (iii) a realistic radiative transfer calculation incorporating as many of the relevant physical process and then would (iv) demonstrate that the the model could produce all of the “important” aspects of high S/N spectra of a group of AGN.

So far, however, most of the attempts to characterize wind features have involved simple applications of phenomenological models contained within XSPEC or SPEX. These models are iteratively fitted to observed data in order to yield values for a small number of free parameters. The models are designed for flexibility, i.e. to be applicable to a wide range of possible geometries, densities, elemental abundances, etc. A goal is to establish conditions in warm absorbers, for example to estimate the amount of reflection from the disk, or to determine ionization conditions. These models typically incorporate substantial detail in the synthesis of the spectrum, in order to provide the maximum realism if their assumptions are correct. For example, models for the X-ray spectrum radiated by a plasma in coronal equilibrium, or models for the X-ray opacity of a photoionized plasma, typically include potential contributions from  $\sim 10^5$  lines or edges from  $\sim 10^2 - 10^3$  ions. On the other hand, they ignore or simplify fundamental questions associated with the geometry and dynamics

of the gas. Therefore the failure of such a model to provide a satisfactory or plausible fit is a likely indicator of the breakdown of one or more of the simplifying assumptions.

The lack of detailed modelling reflects both the absence of a consensus on the geometry of AGN and also the limited number of high S/N X-ray spectra of AGN. However, some progress toward the goal of a consistent physical model for AGN outflows is being made. For, example, Schurch & Done (2007) and more recently by Saez & Chartas (2011) treat the wind essentially as a 1-d outflow, which is reasonable if one is only interested in the shape of the absorption. They define the wind in terms of a series of shells of varying velocity, with distribution based on physically consistent dynamical models. They calculate the state of the gas in and the transmitted spectrum in each shell sequentially using XSTAR or CLOUDY, modifying the input spectrum in the next shell to allow for changes in velocity, and in this manner create spectra of warm absorbers. Schurch & Done (2007) find they can produce spectra that fit observations of warm absorbers in this manner; Saez & Chartas (2011) find they can reproduce the main characteristics of the ultrafast outflow in APM 08279+5255.

Sim et al. (2008, 2010), by contrast, start with a two-dimensional bi-conical flow. They adopt a kinematic, or parametrized, description of the wind defined in terms of total mass loss, opening-angle, etc., calculate the ionization structure of this wind, and then calculate the X-ray spectrum that would result. They find that with the appropriate choice of parameters, which include mass loss rates comparable to the Eddington accretion rate, that they can reproduce with some precision the shape of the absorption and emission spectrum of Mrk 766 (Sim et al., 2008) and PKS 1211-143 (Sim et al., 2010). Interestingly, these spectral simulations show a redward wing on Fe  $K\alpha$ , without including gravitationally-redshifted fluorescence from from a disk. Instead, the redward wing of Fe  $K\alpha$  arises directly from the scattering from the receding portion of the wind. Tatum et al. (2012) have used XSPEC and a small grid of models created with this Monte Carlo radiative transfer code to model the spectra of a small sample of Seyfert galaxies observed with *Suzaku*, suggesting that a large fraction of the X-ray flux in these AGN is processed by the wind. Whether these types of wind are like those that are found in AGN remains controversial (see, e.g Reynolds, 2012, for a rejoinder on the physical underpinnings of these types of winds). However, similar profiles are produced directly from Kurosawa & Proga (2009) 3-d hydrodynamical simulations (Sim et al., 2012).

Sim et al. (2008, 2010) envision the wind as arising from the accretion disk, at a distance of  $10^{14}$  cm, however an alternative view is that the wind associated with the warm absorber arises from the region of the torus, at a distance of order  $10^{18}$  cm from the BH, the same torus that is believed to obscure the broad line region in Seyfert II galaxies (Krolik & Kriss, 1995, 2001). Dorodnitsyn et al. (2012), for example, have recently calculated 3-d hydrodynamical models showing that a bi-conical flow is generated by the intense flux of X-rays at the inner edge of the torus showing that these flows can generate absorption that resembles that observed from warm absorbers in Seyfert I galaxies. Typical mass loss rates of range from about  $10^{-2}$  to  $10^{-1} M_{\odot} \text{ yr}^{-1}$  and velocities of the outflowing gas are typically 100-1000 km  $\text{ s}^{-1}$ . While detailed fits to existing X-ray spectra of systems have not been attempted (no doubt in part because the outflow is not steady), this is just a matter of time.

### 3.2 Prospects & Strategy

The most widely applied models are based on extremely simple assumptions about the more fundamental physical quantities which affect the observations. For example, time-steady equilibrium is assumed in the most widely applied models, and a single value of the most important free parameters (eg. temperature, ionization balance) is specified rather than a distribution. The failure of such a model to provide a satisfactory or plausible fit is therefore a likely indicator of the breakdown of one or more of these assumptions. In this sense, many or all *ASTRO-H* observations will include the testing of numerical models. This type of model testing is not unique to *ASTRO-H*, though it is likely that *ASTRO-H* will provide new tests or results of this type owing to its new capabilities.

An additional sense in which numerical models can be tested is that observations using other observatories have derived parameter values which fit adequately, and *ASTRO-H* can test whether comparable fits are obtained with these same parameter values. This is new in the sense that *ASTRO-H* is likely to produce higher signal-to-noise and higher spectral resolution data than previous observatories at energies greater than 3–5 keV. For

example, the *Chandra* HETG spectra of bright Seyfert galaxies such as NGC 3783 and MCG –6-30-15 appear to be dominated by warm absorbers, and the spectra fit adequately to several ionization parameter components (Krongold et al., 2003; Holczer et al., 2010). These warm absorber components may be associated features near the iron K lines, and these can be searched for using *ASTRO-H*.

More interesting is that *ASTRO-H* may allow testing of models which include more realistic treatments of the dynamics and geometry of the outflow. The list of such models includes those mentioned in the previous subsection, plus the following:

1) Models for the time variability of the warm absorber, specifically for one case where a detection of correlated variability using *XMM-Newton* has been claimed: NGC 4051 (Krongold et al., 2007). Detection of variability depends on a certain amount of luck, associated with catching a continuum variability event. Although there is no specific prediction for the variability in the iron band, it seems likely that more highly ionized material would be associated with more rapid variability than for the material responsible for the O, Ne, and Fe L absorption. Certainly, detection of variability near the iron K lines on time scales longer than claimed from *XMM-Newton* in this object, or a strong upper limit to variability on the *XMM-Newton* time scale, would represent a strong test of the model advanced for the warm absorber in NGC 4051 by Krongold et al. (2007).

2) Models which consider details of the 'geometry' of the material responsible for X-ray spectral features, i.e. those of Sim et al. (2010, 2012). These models make specific predictions for the iron K region, such as the presence of apparent UFO features.

3) It has been suggested that warm absorbers can mimic the apparent relativistically broadened iron lines in objects such as MCG –6-30-15 (Miller et al., 2009). If so, narrow features associated with highly ionized iron are likely and should be detectable with *ASTRO-H*.

4) Holczer et al. (2007) suggest that the ionization parameter distribution of warm absorber gas is determined by the effects of thermal instability. If so, there should be additional material at ionization parameters greater than have been previously detected, since this gas will be even more thermally stable than the material detected so far. Such material will be observable primarily in iron, since it is more resistant to ionization than other abundant elements. *ASTRO-H* will detect or constrain the existence of this gas, and so indirectly test the thermal instability hypothesis.

### 3.3 Targets & Feasibility

AGN targets which will lend themselves to model testing are generically those for which the data will have the best signal-to-noise ratio in the energy band most favourable to *ASTRO-H*, i.e. the region of maximum SXS sensitivity above 5 keV. These include the well known targets which are already listed as likely targets and have been simulated elsewhere in this white paper, such as MCG –6-30-15 and NGC 3783 (Sect. 1.3.2) and NGC 5548 (Sect. 1.3.3).

## 4 Other types of sources with potential (narrow-band) outflow features

### 4.1 Background and Previous Studies

#### 4.1.1 BAL quasars

Some quasars (QSOs) show fast outflowing gas features in their UV spectra. The measured line blue-shifts well exceed  $1000 \text{ km s}^{-1}$  and can be as large as  $\sim 3-6 \times 10^4 \text{ km s}^{-1}$  ( $\sim 0.1-0.2c$ ). Depending on the intrinsic velocity width of the lines, these QSOs are classified as broad absorption line (BAL;  $\text{FWHM} > 2000 \text{ km s}^{-1}$ ), mini-BAL ( $500 \text{ km s}^{-1} < \text{FWHM} < 2000 \text{ km s}^{-1}$ ) and narrow absorption line (NAL;  $\text{FWHM} < 500 \text{ km s}^{-1}$ ). In the X-rays BAL QSOs are intrinsically weak and only for a few sources it has been possible to perform a detailed spectral analysis (e.g., Chartas et al., 2002). On the other hand, Mini-BAL QSO are a more promising class of sources as they display a higher flux which translates in a higher quality X-ray spectrum. From the few examples we know, these objects have complex spectra, characterized by multicomponent warm absorbers, often with large

column density and outflowing at high velocity. Also ultra-fast-outflows have been reported for some of these sources (Giustini et al., 2011).

#### 4.1.2 Partially covered sources

Partially covered sources have been routinely detected and studied with current instruments. The nature of the coverer is in general not known. Degeneracy exists between a partial covering model and a reflection model, which can mimic the same spectral shape, especially below 10 keV. A higher energy coverage is of great help in trying to disentangle between the two scenarios. In some sources, for example NGC 1365 (Risaliti, 2009), Mrk 766 (Miller et al., 2007), one or more partial covering layers of gas have been claimed. The ionization structure of these partial covering clouds is complex and sometimes they have been observed through eclipses of the X-ray source. During the occultation from the cloud, a cold absorber is often associated with a highly ionized gas (e.g., Fe XXV and Fe XXVI), possibly suggesting a cometary structure. The study of the several layers which (temporarily) obscure the source is important for understanding the geometry of the gas around the black hole and how the gas layers are shielding each other from the primary radiation. This can provide an important observational benchmark for theoretical models of accretion disk winds (e.g. launching and heating mechanisms).

#### 4.1.3 Compton thick outflows

A related topic to partial covering sources and ultra-fast outflows is that of Compton thick absorbers. In some remarkable sources, such as PDS 456, a Compton thick absorber has been detected. This source is classified as a classical Seyfert 1 galaxy (i.e. not a BAL QSO or a Seyfert 2). The absorber displays very deep features from highly ionized iron possibly with multiple velocity components. The features indicate that the gas is outflowing from the nucleus of this galaxy at the relativistic speed of  $\approx 0.3 c$ . These outflows possibly originate from the accretion disk itself and can have important consequences in evaluating the feedback from quasars. Indeed, as shown in Equation (1), the kinetic luminosity carried by this plasma is a strong function of the outflow velocity ( $\propto v^3$ ) and linearly dependent on the column density ( $N_{\text{H}} \sim 10^{24} \text{ cm}^{-2}$  in this object).

## 4.2 Prospects & Strategy

**Table 4:** Possible targets for *ASTRO-H*

Name	type	redshift	EW (FeXXVI) eV	Ref.	Flux <sub>(2–10keV)</sub> erg cm <sup>-2</sup> s <sup>-1</sup>	Ref.
PG 1126-041	miniBAL w UFO	0.06	10.2±0.1	<i>a</i>	3×10 <sup>-11</sup>	2
Mrk 766	PC + HIG	0.013	40–60 FeXXV	<i>b</i>	2×10 <sup>-11</sup>	1
NGC 1365	PC + HIG	0.005	100±60 FeXXVI K $\beta$	<i>c</i>	1.5×10 <sup>-12</sup>	1
PDS 456	CT + UFO	0.184	129±48	<i>d</i>	3.5×10 <sup>-12</sup>	1

Notes:

PC: partial covering; BAL: broad absorption line quasar; UFO: ultra-fast outflow; HIG: highly ionized gas; CT: Compton thick. Fluxes are in erg cm<sup>-2</sup> s<sup>-1</sup>

References for equivalent width (EW): *a* Giustini et al. (2011); *b* Risaliti (2011); *c* Risaliti (2009); *d* Reeves et al. (2009); References for flux measurements: 1: Tartarus data base; 2: Giustini et al. (2011)

The general prospects and strategy for these AGN are very similar to those previously discussed in §1.2 and §2.2 for the ionized gas in “normal” and “ultra-fast” outflows, respectively. In particular, the large effective area above 6 keV will allow to study a series of transitions for each component (e.g. FeXXVI 1s–2p and 1s–3p and the K-edge). This will help in characterizing optically thick plasmas where the main transitions are probably saturated. Plasmas with large column densities do display features in the iron K $\alpha$  region even for low values

**Table 5:** Parameters for PG 1126-041. Column densities are in units of  $\text{cm}^{-2}$ , velocities in  $\text{km s}^{-1}$  and fluxes in  $\text{erg cm}^{-2} \text{s}^{-1}$ .

$N_{\text{H}}^1$	$1.48 \times 10^{23}$
$\xi^1$	1.66
$N_{\text{H}}^2$	$7.5 \times 10^{23}$
$\xi^2$	3.4
$v_{\text{out}}$	-16200
$F_{0.2-10\text{keV}}$	$8.5 \times 10^{-11}$
<b>Results:</b>	
$N_{\text{FeXXV}}$	$1.23 \pm 0.24 \times 10^{19}$
$N_{\text{FeXXVI}}$	$2.7 \pm 1.1 \times 10^{18}$

of the ionizing parameter (e.g. lines from Fe XVIII-Fe XXII). Therefore, this spectral region is then crucial for disentangling the different gas components. The broad-band coverage and high effective area of *ASTRO-H* will be very important to distinguish between reflection and partial covering models (overlap with science case of reflection in AGN). Finally, time-resolved or monitoring studies will be fundamental for the determination of the covering fraction as a function of time and for possible occultation events, such as X-ray eclipses.

### 4.3 Targets & Feasibility

#### 4.3.1 BAL QSOs

We present here a simulation for PG 1126-041. The required exposure time to detect Fe XXV at  $5\sigma$  is 400 ks. The input parameters for the simulation come from Giustini et al. (2011). These consist of a double powerlaw, one of which is absorbed by two gas components. See Table 5 and Figure 11.

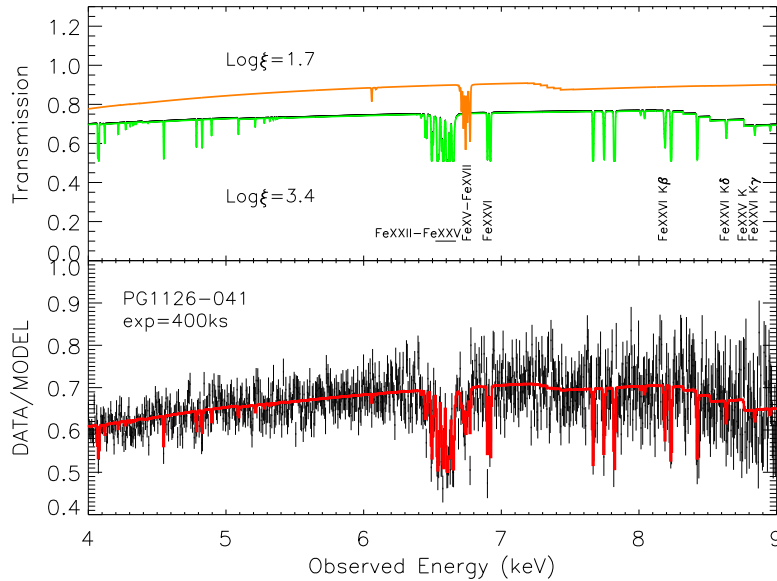


**Figure 11:** Simulated spectrum of PG 1126-041 for a 400 ks observation.

#### 4.3.2 Compton thick outflows

PDS 456 ( $z = 0.184$ ) has been well known as the most luminous AGN ( $L_{\text{bol}} \sim 10^{47} \text{ erg s}^{-1}$ ) in the local universe. In spite of the fact that more luminous AGNs tend to show less variability in the X-ray band, PDS 456 exhibits



rapid and large amplitude flux variation accompanied by the spectral changes on time scales of hours to years. Figure 12, which is referred from Behar et al. (2010), shows the various spectra of PDS 456 observed by several X-ray satellites. Each spectrum is divided by a power-law with  $\Gamma = 2$  absorbed by Galactic column.

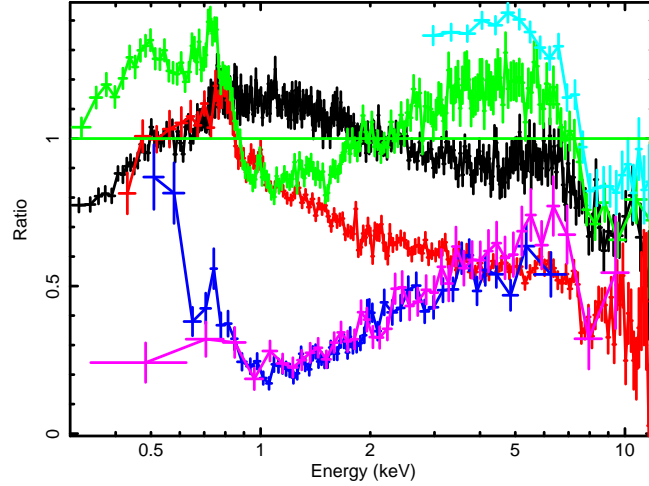


**Figure 12:** Various spectral state of PDS 456 (Behar et al., 2010). *XMM-Newton* observation in 2007 (black), *Suzaku* in 2007 (red), *XMM-Newton* in 2001 (green), *Chandra* in 2003 (blue), *ASCA* in 1998 (magenta), and *RXTE* in 2001 (cyan).

*ASCA* and *RXTE* observations revealed the presence of a strong edge-like feature in the iron K-shell band (Reeves et al., 2000). Reeves et al. (2003) reported the detection of blueshifted ( $\sim 50\,000\text{ km s}^{-1}$ ) iron K-shell absorption features based on the spectrum obtained from the *XMM-Newton* observation in 2001. Furthermore, *Suzaku* observation in 2007 also revealed the significant absorption features near 9 keV in the source rest frame (Reeves et al., 2009). If this absorption is due to blueshifted resonance transition of hydrogen-like iron, then the outflow velocity reach nearly 30% of the speed of light.

In this subsection, we present the results on the SXS simulation based on the *Suzaku* spectrum obtained in 2007. An unprecedented energy resolution of SXS in the iron band allows us to strictly determine the outflow velocity, ionization states and the column density of the gas.

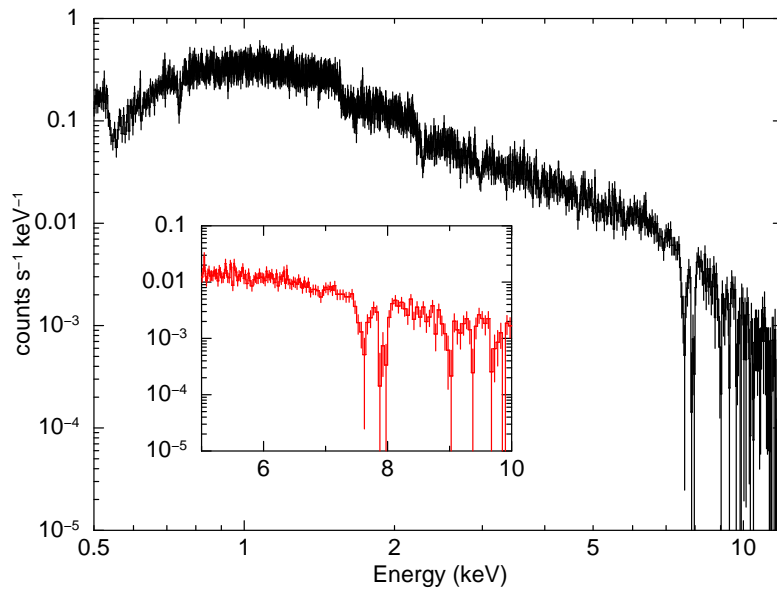


**Figure 13:** Simulated spectrum of PDS 456 for 100 ks exposure. The inset shows an enlargement of the iron line region.

Figure 13 shows the simulated spectrum with 100 ks exposure. We used the redistribution matrix function

(RMF) with 5 eV resolution, which is the current best-estimated version (ah\_sxs\_5ev\_basefilt\_20100712.rmf), and the ancillary response file (ARF) for the point source (sxt-s\_120210\_ts02um\_intallpxl.arf). The assumed model function is as follows:

$$F(E) = \exp(-\sigma(E)N_{\text{H}}^{\text{Gal}}) \times (\text{WA}(\xi_{\text{WA}}, N_{\text{H}}^{\text{WA}}, v_{\text{out}}) \times A_{\text{pl}}E^{-\Gamma} + \text{REF}(\xi_{\text{REF}}, A_{\text{REF}})), \quad (11)$$

where WA and REF mean the absorption by warm absorber (XSTAR analytic model, WARMABS in XSPEC) and the ionized reflection component (REFLIONX in XSPEC; Ross & Fabian, 2005; Ross et al., 1999), respectively.  $N_{\text{H}}^{\text{Gal}}$  and  $N_{\text{H}}^{\text{WA}}$  represent the column density of Galactic and warm absorber, respectively. The ionization parameters of the absorber and the reflector are expressed as  $\xi_{\text{WA}}$  and  $\xi_{\text{REF}}$ , respectively.  $v_{\text{out}}$  is outflow velocity of the absorber, and the turbulent velocity of the absorber was assumed to be 2 500 km s<sup>-1</sup> according to Behar et al. (2010).  $A_{\text{pl}}$  and  $A_{\text{REF}}$  are normalization of power-law and reflection components, respectively. The assumed parameters are summarized in Table 6.

**Table 6:** Parameters in the simulated spectrum of PDS 456

$N_{\text{H}}^{\text{Gal}}$ 10 <sup>21</sup>	$\log \xi_{\text{WA}}$ erg s <sup>-1</sup> cm	$N_{\text{H}}^{\text{WA}}$ 10 <sup>24</sup> cm <sup>-2</sup>	$v_{\text{out}}$ km s <sup>-1</sup>	$A_{\text{pl}}$	$\Gamma$	$\log \xi_{\text{REF}}$ erg s <sup>-1</sup> cm	$A_{\text{REF}}$
2.1	3.5	1.0	90,000	$3.1 \times 10^{-3}$	2.25	3.0	$3 \times 10^{-9}$

In order to estimate the significance of the absorption feature, we fitted the 5–10 keV spectrum with a single power-law and two negative Gaussian models. Figure 14 upper panel shows the data (black) and model (red) we applied, and the residuals are represented in the lower panel. Fitting results are summarized in Table 7. Both lines can be detected at highly statistically significance level ( $> 5\sigma$ ). If these lines are identified as H- and He-like iron, then the outflow velocity can be determined to be  $34.4 \pm 0.3\%$  of speed of light.

**Table 7:** Parameters in the simulated spectrum of PDS 456

(1)	(2)	(3)	(4)	(5)	(6)	(7)	(8)
$E_1$	$\sigma_1$	$F_1$	$EW_1$	$E_2$	$\sigma_2$	$F_2$	$EW_2$
$9.37 \pm 0.02$	$90_{-7}^{+13}$	$-4.9_{-0.4}^{+1.0}$	$0.25_{-0.02}^{+0.01}$	$9.01 \pm 0.02$	$101_{-11}^{+28}$	$-5.3_{-0.5}^{+0.8}$	$0.24_{-0.04}^{+0.03}$

Notes:

(1),(5); line center energy at the source rest frame in unit of keV.

(2),(6); line broadening in unit of eV.

(3),(7); line flux in unit of  $10^{-6}$  photons cm<sup>-2</sup> s<sup>-1</sup>.

(4),(8); line equivalent width in unit of keV. Errors on the equivalent width are quoted at 68% confidence.

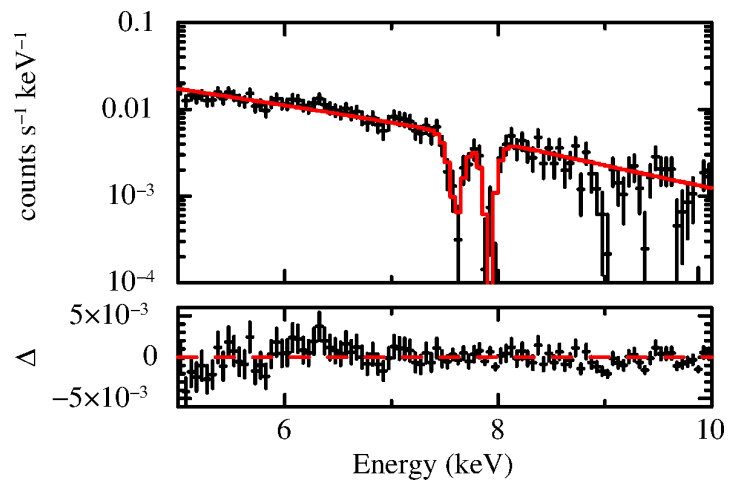


**Figure 14:** 5–10 keV spectrum of PDS 456 fitted with a single power-law and two negative Gaussians.

## References

- Ashton, C.E., et al. 2006, MNRAS, 366, 521
- Behar, E. 2009, ApJ, 703, 1346
- Behar, E. 2010, ApJ, 712, 26
- Bianchi, S., et al. 2010, A&A, 522, A64
- Blustin, A.J., et al. 2005, A&A, 431, 111
- Cappi, M., et al. 1999, A&A, 344, 857
- Cappi, M. 2006, AN, 327, 1012
- Cappi, M., et al. 2009 A&A, 504, 401
- Chartas, G., et al. 2002, ApJ, 579, 169
- Chartas, G., et al. 2003, ApJ, 595, 85
- Chatterjee, R., et al. 2009, ApJ, 704, 1689
- Chatterjee, R., et al. 2011, ApJ, 734, 43
- Crenshaw, D.M. & Kraemer, S.B. 2012, ApJ, 753, 75
- Detmers, R.G., et al. 2011, A&A, 534, A38
- Dorodnitsyn, A., Kallman, T., & Bisnovatyi-Kogan, G. S. 2012, ApJ, 747, 8
- Fischer, T.C., et al. 2012, ASP Conf. Ser. 460, 154
- Fukumura, K., et al. 2010, ApJ, 715, 636
- Giustini, M., et al. 2011, A&A, 536, 49
- Gofford, J. et al. 2012, arXiv:1211.5810
- Halpern, J.P. 1984, ApJ, 281, 90
- Holczer, T., Behar, E., & Kaspi, S. 2007, ApJ, 663, 799
- Holczer, T., Behar, E., & Arav, N. 2010, ApJ, 708, 981
- Hopkins, P.F. & Elvis, M. 2010, MNRAS, 401, 7
- Kaastra, J.S., Mewe, R. & Nieuwenhuijzen, H. 1996, 11th Coll. UV & X-ray Spectr. Astrophys. & Lab. Plasmas, p. 411
- Kaastra, J.S., et al. 2000, A&A, 354, L83
- Kaastra, J.S., et al. 2002, A&A, 386, 427
- Kaastra, J.S., et al. 2002, A&A, 539, A117
- Kallman, T. & Bautista, M. 2001, ApJS, 133, 221
- Kaspi, S., et al. 2000, ApJ, 535, L17
- King, A.R. 2010, MNRAS, 402, 1516
- King, A.R. & Pounds, K.A. 2003, MNRAS, 345, 657
- King, A.R., et al. 2013, ApJ, 762, 103
- Kraemer, S.B., et al. 2005, ApJ, 633, 693
- Krolik, J.H., & Kriss, G A. 1995, ApJ, 447, 512
- Krolik, J.H., & Kriss, G.A. 2001, ApJ, 561, 684
- Krongold, Y., et al. 2003, ApJ, 597, 832
- Krongold, Y., et al. 2007, ApJ, 659, 1022
- Longinotti, A.L., et al. 2009, MNRAS, 394, L1
- Kurosawa, R., & Proga, D. 2009, ApJ, 693, 1929
- Matt, G., et al. 2006, A&A, 445, 451
- McKernan, B., et al. 2007, MNRAS, 379, 1359
- Miller, L., et al. 2007, A&A, 463, 131
- Miller, L., Turner, T.J., & Reeves, J.N. 2009, MNRAS, 399, L69
- Neilsen, J. & Lee, J.C. 2009, Nature, 458, 481
- Netzer, H., et al. 2003, ApJ, 599, 933
- Ohsuga, K., et al. 2009, PASJ, 61, L7
- Pounds, K.A., et al. 2003, MNRAS, 345, 705
- Reeves, J.N., et al. 2000, MNRAS, 312, L17
- Reeves, J.N., et al. 2003, ApJ, 593, L65
- Reeves, J.N., et al. 2004, ApJ, 602, 648
- Reeves, J.N., et al. 2009, ApJ, 701, 493
- Reynolds, C.S. 1997, MNRAS, 286, 513
- Reynolds, C.S. 2012, ApJL, 759, L15
- Risaliti, G., et al. 2009, ApJ, 696, 160
- Risaliti, G., et al. 2011, MNRAS, 410, 1027
- Ross, R.R., Fabian, A.C., & Young, A.J. 1999, MNRAS, 306, 461
- Ross, R.R. & Fabian, A.C. 2005, MNRAS, 358, 211
- Schurch, N.J. & Done, C. 2007, MNRAS, 381, 1413
- Saez, C. & Chartas, G. 2011, ApJ, 737, 91
- Sim, S.A., Long, K.S., Miller, L., & Turner, T.J. 2008, MNRAS, 388, 611
- Sim, S.A. et al. 2010, MNRAS, 404, 1369
- Sim, S.A., et al. 2012, MNRAS, 426, 2859
- Steenbrugge, K.C., et al. 2005, A&A, 434, 569
- Tatum, M.M., et al. 2012, ApJ, 752, 94
- Tombesi, F., et al. 2010a, A&A, 521, A57
- Tombesi, F., et al. 2010b, ApJ, 719, 700
- Tombesi, F., et al. 2011, ApJ, 742, 44
- Tombesi, F., et al. 2012, MNRAS, 422, L1
- Tombesi, F., et al. 2013, MNRAS, 430, 1102
- Turner, T.J., et al. 2008, A&A, 483, 161
- Yaqoob, T., et al. 2005, ApJ, 627, 156
- Young, A.J., et al. 2005, ApJ, 631, 733